Dimensional Tailoring of Hybrid Perovskites for Photovoltaics

Giulia Grancini* and Mohammad Khaja Nazeeruddin*

Group for Molecular Engineering of Functional Materials, Institute of Chemical Sciences and Emngineering, Ecole Polytechnique Fédérale Lausanne Valais Wallis, CH-1951 Sion, Switzerland.

*Email: giulia.grancini@epfl.ch; mdkhaja.nazeeruddin@epfl.ch

Abstract. Hybrid perovskites have been recently listed as one of the most attractive fields of research of our time, given their enormous demonstrated potential in optoelectronics, and photovoltaics. Three dimensional hybrid perovskites (3DP) in the form of organic-inorganic metal-halide structure have been in photovoltaic scene owing to their unique optoelectronic properties leading to high power conversion efficiency (PCE) along with their low-cost and scalable solution-based fabrication processes[1–4]. However, their market exploitation is still inhibited by their inherently poor stability (i.e., product lifetime), due to their ease of degradation when exposed to moisture[3–6]. In this review, we focus on a different class of hybrid perovskites materials which self-assembles into a low dimensional structure, i.e., two-dimensional perovskite (2DP). Based on alternating organic – inorganic layers, similar to a hybrid quantum well system, their inherent versatile structure enables the fine tuning of their optoelectronic properties, with a large scope for many different optoelectronic applications[7–10]. Their highest value relies on their superior moisture stability, far beyond the one of standard 3DP, forecasting to be the ideal solution for stable photovoltaic devices[11–13]. Being the 2DP field still at its infancy, several prominent topics on 2DP, such as design, fabrication, and incorporation into working devices, are subject of intense ongoing research and will be discussed in the following in more details. The most common 2DP will be described with a special focus on chemical structure, material engineering aspects and optical and photophysical behavior. Importantly, we will review their main use as a "stabilizer" agent in the active layer of perovskite solar cell. In a synergic action with 3DP boosted device efficiency and stability are demonstrated, paving the way for a new era of mixed dimensional perovskite solar cells for market applications.

1. Introduction: from 3D to 2D hybrid perovskites

In the last years, the photovoltaic (PV) science has witnessed the ascent of a new contender which promises efficient and cheap solar energy using solution-processable hybrid semiconductors in the form of organic - inorganic halide perovskites. In less than a decade, perovskite research is taking over

the academic and industrial interest with their solar to electricity PCE nowadays surpassing 22%, comparable with commercially available solar technologies[1,3,5]. The most known hybrid perovskite, i.e. methylammonium lead-iodide ($CH_3NH_3PbI_3$) as test-bed system, consists of a three-dimensional (3D) network arranging into an ABX_3 structure, where A is the organic cation (i.e. MA=$CH_3NH_3^+$), B the metal cation (i.e., Pb^{2+} or Sn^{2+}), and X the halide anion (i.e., Cl^-, Br^-, I^-) (Figure 1a)[3,14]. Notably, the size of the A cations must be small enough to fit within the voids of the octahedral unit (Figure 1), keeping the structural integrity of the 3D lattice. The limit in the size of the A cation is 2.6A as dictated by the empirical *Goldschmidt tolerance* factor. This drastically reduces the possible choice of organic cations that can form a 3D lattice to only a few[3,15]. Behind the exceptional performances, 3DPs hold unique electrical and optical properties manifested as the high absorption coefficient, direct photo-generation of free carriers, efficient charge transport, and long carrier diffusion lengths, to mention a few[16]. Another striking attribute is their high defect tolerance despite being deposited from solution, which results in high open-circuit voltage (V_{OC}) exceeding 1V, approaching the same level of photon energy utilization as the solar technologies now on the market[14]. Typical perovskite solar cells (PSCs) exploit a sandwich configuration where the perovskite is embedded between an electron transport layer (ETM), such as the mesoporous titanium dioxide (TiO_2) or tin dioxade (SnO_2), and an organic hole transporting material (HTM), such as spiro-OMeTAD or polymeric PTAA in either a *n-i-p* or *p-i-n* (inverted) device architectures[3,5]. The full potential of this technology and the big excitement that came along has been recently more and more questioned by their relatively poor stability (short lifetime) which affect device under operative conditions[5,6,11,17,18]. Perovskite devices currently last for few months outdoors, whereas, a warranty for at least twenty-five years is requested for a marketable product. To overcome the stability issues, material compositional engineering, introduction of moisture-resistant layers, additives and ionic liquid and the design of alternative device architectures have been explored so far, leading to a certain extent to some incremental improvements[18–21]. By contrast, their parent low dimensional perovskites, arranging in the 2D, so-called *Ruddlesden–Popper*-phase, have demonstrated higher environmental stability[9,11,13], paving the way for their possible integration in working device as a "stabilizer" component. The research in this field, mainly devoted to the combination of 2DP and 3DP into hybrid composites, has literally exploded in the last year, making the way to the market closer. Ideally, 2DP can be structurally obtained by slicing the 3D frameworks along specific crystallographic planes, resulting in single (or multiple) inorganic sheets, sandwiched in between the organic cation layers[8,10,22–24]. The layers are held together by Coulombic force, which maintain the structural integrity. The 2DP has a general formula $\mathbf{R_2(A)_{n-1}B_nX_{3n+1}}$ **(n=1, 2, 3, 4, …)**, where **R** is the bulky organic molecule (such as an aliphatic or aromatic alkylammonium cation, i.e. 2-phenylethylammonium (PEA) or n-butylammonium (n-BA)), acting as a spacer between the

inorganic sheets (Figure 1b)[8,22,24]. **A** is the monovalent organic cation, i.e. $CH_3NH_3^+$ (MA^+) and $HC(NH_2)_2^+$ (FA^+), **B** the divalent metal and **X** the halogen and *n* the number of the inorganic layers within each quantum well (Figure 1). If *n=1* (Figure 1b) the structure reads as $\mathbf{R_2BX_4}$: organics isolate single layers of the inorganic framework in a pure 2DP phase. On the other side, increasing the number of layers (*n>1*) (Figure 1b) and adding another small organic cation (**A**) induces the formation of multi-layered *quasi-2D* perovskites converging into the 3D structure for $n=\infty$[8,9,22]. From an optoelectronic perspective, the main character of this material is the confinement of a stable exciton due to the dielectric mismatch and low dielectric screening from the organic sheets, resulting in a larger binding energies (Figure 1c). Interestingly, exciton binding energy progressively decreases upon increasing *n* as going from a 2DP to a 3DP. Such structural tunability directly impacts on the device functions[9,22,24]. For instance, when $n\leq2$, the perovskites exhibit strong photoluminescence (PL) at room temperature, implying they can be suitable for the use in light emitting devices (LEDs)[25,26]. At the same time, the narrow absorption and high exciton binding energy that asks for an extra energy to be dissociated, leading to a significant loss-in-potential, are not ideal attributes for photovoltaics. For the 2DP with $n \geq 3$, their low exciton binding energy and strong light absorption in the visible region (Figure 1), suggest their good potential for solar cells. In this case, excitons can be dissociated at room temperature and they can work as active layer in a solar cell device leading to PCE=15% (for high n, such as n=60)[27]. The large structural flexibility which can direct the device application, is intimately related to the layered structure of the 2DP which, opposite to the 3DP, allows for a large/bulky cation to be accommodated in between the inorganic sheet, relaxing the *Goldschmidt tolerance rule* for 3D.[15,28,29] Therefore, a wide choice of organic cations becomes available and can even be designed with desired properties and functions, engineered "ad hoc" according to the specific optoelectronic application. To the extreme, π-conjugated structure can be also incorporated, which, being photoactive, can actively participate in the optoelectronic properties of the 2D material. Phosphorescence has been for instance observed in a 2D based on naphthylmethyl cation upon efficient energy transfer happens from the inorganic layer.[23,30–32]

This review will first describe the family of 2DP (n=1) focusing on their chemical and material engineering aspects, along with a discussion on their structural, optical and photophysical properties. Secondly, we will present more in details the properties of *quasi-2D* (n>1), which can be considered as intermediates in between 2DP and 3DP with combined optoelectronic properties. Then, we will highlight the advances made when 2D or quasi-2D perovskites are used in a mixed configuration with 3DP, allowing for layered 2D/3D and mixed 3D/2D novel solar cell designs. Solar cell architectures and their performance are reviewed with a special attention on the role of 2D in stabilizing the device performances.

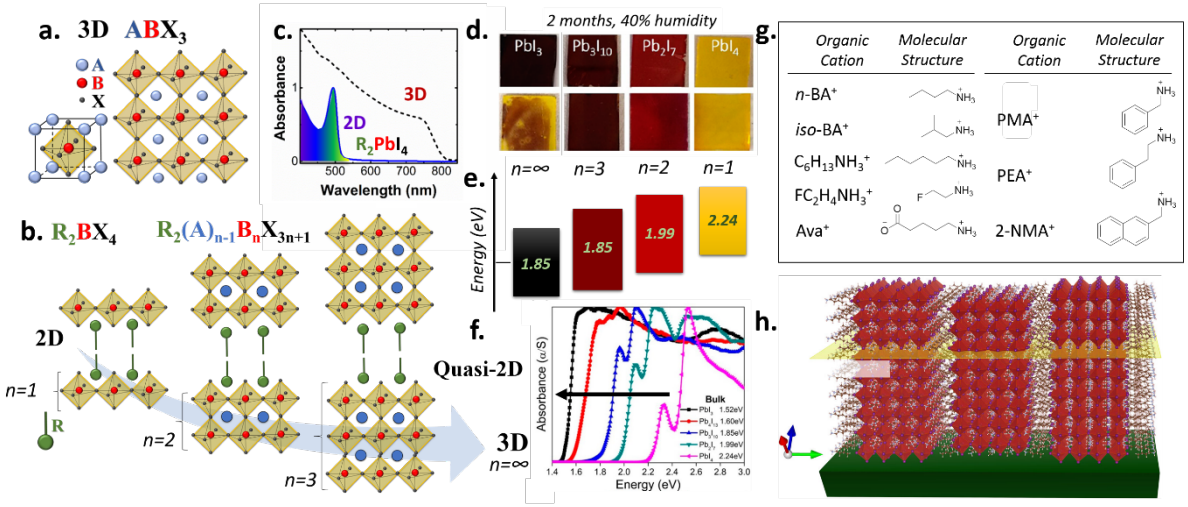

Figure 1. Structure and optical properties of 2D perovskites. a. Cartoon of the 3D Hybrid Perovskite structure showing the PbI_6 octahedra; **b.** Low dimensional perovskite structure from pure 2D, forming a R_2BX_4 structure (n=1) to quasi-2D arranging into a $R_2An\text{-}1B_nX_{3n+1}$ structure with n=2 and n=3. **c.** Absorption spectra of a 2D perovskite compared with a standard 3D perovskite. **d.** Picture of 3D and 2D perovskites (with decreasing n) upon exposure for 2 months under 40% humidity conditions. **e.** Scheme of the energy levels and band gap of PEA_2PbI_4 and quasi 2D $(PEAI)_2(MA)_{n-1}Pb_nI_{3n+1}$. Data extracted from [Cao et al. J. Am. Chem. Soc. 2015, 137, 7843]. **f.** Absorption spectra of quasi 2D $(PEAI)_2(MA)_{n-1}Pb_nI_{3n+1}$ perovskite. Data extracted from [Cao et al. J. Am. Chem. Soc. 2015, 137, 7843]. **g.** Series of organic cations with their molecular structure generally used to form 2D perovskites. **h.** Illustration of an orthorhombic (101) vertically oriented 2D perovskite structure, with (202) planes parallel to the substrate. Figure from [Chen et al. Nat. Commun. 2018, 9, 1336].

2. Low dimensional perovskites

2.1 Structural and Optoelectronic Properties

As mentioned above, given the relaxed steric constrains imposed on the organic cations by the empirical *Goldschmidt's tolerance factor rule*, 2DPs provide a large scope for material exploration and compositional engineering. Figure 1g shows few examples of the most used ones. Phenylethylammonium (*PEA*) and -butylammonium (*n-BA*) are for instance ones of the most explored cations in the last couple of years. PEA_2PbI_4 (n=1 where PEA alternates monolayer of the inorganic backbone) has been first developed in the early '90s [33,34], and nowadays widely studied as a test-bed material to shed light on the structural and optoelectronic properties of the entire class of 2DP. A common for 2DP, PEA_2PbI_4 shows a large band gap, around 2.24 eV (Figure 1e) and a high exciton binding energy up to 220 meV responsible for their excitonic behaviour[27,29]. This results in interesting

optoelectronic properties such as high electroluminescence, high photoluminescence quantum yield (PLQY) and strong optical non-linearity. If mixing PEA with a smaller cation, i.e. MA, a $PEA_2(MA)_{n-1}Pb_nI_{3n+1}$ structures are formed, where the thickness of the inorganic sheet can be tuned to bilayer (*n=2*), three layers (*n=3*) and even multiple layers by the addition of the MA in a proper stoichiometric ratio. These compounds are referred as *quasi-2D* perovskite (Figure 1b). Increasing the number of layers (*n*) the band gaps change progressively between 2.57 eV for the *n=1* and 1.50 eV for *n=∞*, [33] and the exciton binding energy reduces[27]. For simplicity, the structure is denoted as Pb_3I_{10}, Pb_2I_7, and PbI_4 when *n* is equal to 4, 3, 2, and 1, respectively. Decreasing n, the optical band gaps of the $(BA)_2(MA)_{n-1}Pb_nI_{3n+1}$ series increases from 1.52 eV (*n = ∞*) to 2.24 eV (*n = 1*), as a result of the quantum confinement effects[8,22]. Tuning *n*, the energetic alignment also changes: in particular, the valence band (VB) maximum increases with decreased dimensionality, from PbI_3 (-5.46 eV) to PbI_4 (-4.55 eV) (Figure 1e). The conduction band (CB) edge also increases in parallel with the VB edge. Notably, as shown in the cartoon in Figure 1e, the CB energy levels lye above the TiO2 CB, enabling electron transfer to the metal oxide, as the typical electron-transport layer used in solar cells architecture. Figure 1f shows the absorption spectra of a family of quasi-2DPs obtained using the *BA* cation and arranging in the form of $(BA)_2(MA)_{n-1}Pb_nI_{3n+1}$. A clear peak close to the band edge is observed, with a remarkable intensity for the *n = 1* which progressively decreases as the number of the inorganic slabs increases and practically disappears for the *n=4* (Figure 1f)[8]. This feature is attributed to a stable excitonic state. This results from dielectric confinement arising from the intercalating organic layers which substantially increases the Coulomb correlations. The localized positively charged BA ions around the negatively charged $(MA)_{n-1}Pb_nI_{3n+1}$ layers can induce a strong local field which screens the charges and thus inhibiting their long-range separation. The strength of the excitonic feature, and thus of the excitonic binding energies decreases with increasing *n* (from 1 to ∞), from hundreds of meV for n=1 down to tens of meV for n>4. The exciton absorption mainly comes from the electronic transition within the inorganic layer, for instance, mainly from Pb(6s)-I(5p) mixed states to Pb (6p) states for lead-based perovskites. In addition, for a fixed halogen, the excitonic peak strongly correlates with the different perovskite lattice distortion (related to the Pb – X – Pb angle). Such structural distortion has been shown to decrease the width of the VB (and CB), leading to a widening of the bandgap and of the exciton binding energies [8,24,35,36]. The tunability in the exciton position (and in the excitonic emission) enables the design of light emitting devices based on 2DP covering the whole visible and near-IR spectral region. Both PMA_2PbI_4 and PEA_2PbI_4, for instance, have been used to fabricate green and violet light emitting devices, respectively[24]. The n value not only influences the optoelectronic properties, but also drives the crystal formation and orientation of 2DP. For instance, the (BA)2(MA)n−1PbnI3n+1 2D perovskite crystals are preferentially aligned parallel to

the substrate if n = 1, while they turn orthogonal to it when n = 4. To simplify, when n is low, the ambient stability is preserved due to the dominant contribution of the hydrophobic spacing cations while the charge carrier transportation is hindered, and vice versa. There is always a trade-off between device performances and stability. For n=1, the presence of the bulky long-chain ensures a surface termination with the organic ligands which, being hydrophobic, impart an additional water-resistant character to the film. As a consequence, 2DP show remarkably improved stability against humidity compared to 3DP. However, as mentioned, the 2DP growth is directed with an orientation parallel to the substrate, as a result from the in plane growth induced by the layered structure.[8] However, for efficient devices, one would desire an alignment of the 2DP layers perpendicular to the electrode layers, ensuring the charge transport through the inorganic layers. It is expected that a vertically oriented 2DP thin film provides direct pathway for electron and hole transport, while the charge transport is hindered by hopping across the long-chain organic surface ligands in a more randomly oriented film (indeed, the bulky organic barriers that separate the 2D metal halide slabs are electrically insulating, preventing charge transport). Thus, for solar cell stack optimization, where the 2DP thin film is sandwiched in between the two electrodes, a vertical alignment of 2DP would be preferable ~~transport~~ (as reported in Figure 1h). However, 2DP forms spontaneously from a simple one-step spin coating deposition of the solution, with a natural tendency to align parallel to the substrate. Indeed, in this case homogeneous nucleation can happen and result in a preferential orientation upon deposition on a substrate due to the 2D crystal preferential orientation that maximizes interactions between the crystals and the substrate, such as van der Waals (vdW) attraction. In this case, an horizontal interaction induces the orientation of the 2D crystal plates. On the other side, vertical alignement should then start from inhomogeneous nucleation. This can happen at the liquid–air interface as recently demonstrated. As shown by grazing incidence wide angle X-ray scattering (GIWAXS), thin films of vertically oriented BA2MA3Pb4I13 crystals can be formed, originated from the anisotropic environment of liquid–air interface. This is likely due to surface tension which makes nucleation and growth at the liquid–air interface of perovskite precursor solution more favourable. As a consequence of the top-down growth mechanism, high-quality 2DP thin films can be deposited on various substrates ranging from polymers to metal oxides. With this method, as described more in details in Section 4.1. enables the realization of high efficient 2DP solar cells. This offers an example, showing the huge actual interest in the rationalization of the design guidelines to obtain a vertically stacked 2DP. To this regard, recently, Tsai et al. reported a full understanding of the charge transport mechanisms in2DP, showing that dominant photocurrent collection is limited by electric field-assisted electron–hole pair separation and transport across the organic barriers. More in details, up to a threshold thickness of 200 nm, at which the absorption is maximized, the photogenerated carrier

separation and transport are highly efficient assisted by the strong internal electrical field. Beyond, the recombination increases significantly. Electronic transport is found to be thermally activated, suggesting that charge carriers need to surmount potential barriers before they are collected at the contacts. These barriers could originate from the presence of imperfect stacking of the inorganic slabs in thin films, which may introduce organic spacers that intermittently disrupt the conducting pathway leading to field-dependent charge collection, independently from the nature of the photogenerated carrier (exciton or free carrier). To limit recombination losses of charge carriers, long-range vertical packing must be targeted to enhance charge conduction. Alternatively, doping the organic spacers to reduce the dielectric contrast could also lower the potential barriers. Further work has to be done in order to address this actual challenge.Before concluding this section, it is worth mentioning that controlling 2DP doping level, is essential for determining the charge carrier and defect density and controlling the band alignment and device operation. In solution-processed semiconductors, as 3DP, defects including interstitials and vacancies with shallow energy levels are generally present. Self-doping in single crystals of 2DP in the form of PEA2PbI4· (MAPbI3)n−1 (PEA, phenethylammonium; MA, methylammonium; n = 1, 2, 3), representative case for 2DP, has been recently investigated. Surprisingly, the authors found, by measuring the sheet conductivity, an extremely low self-doping concentrations in the 2DP crystals, over three orders of magnitude lower than those of typical 3DP (such as MAPbI3 and MAPbBr3). The reduced self-doping level with the reduced crystal dimensionality has been assigned to a defect-suppressing crystallization process mediated by the large organic cations. As a result of the low equilibrium carrier concentration, electronic noise in preliminary PEA2PbI4·(MAPbI3)n−1 (n = 1, 2, 3) single crystal-based photoconductors markedly diminishes, giving rise to extraordinarily high light detectivity.**2.2. Excited state physics in 2D hybrid perovskites.**

Understanding the exciton dynamics in 2DP is crucial to both fundamental knowledge as well as to drive an intelligent device design and optimization. If we compare them to conventional inorganic semiconductor layered system (i.e. quantum wells -QWs), such as the prototypical III−V GaAs junction, the 2DPs are obtained by simple deposition process which leads to more “jelly-like” material structure which is able to accommodate structural distortions, leading to a higher degree of local disorder.[37,38]. In inorganic QWs, for instance, Anderson localization that is a structural disorder which can lead to exciton localization, is happening [39]. On the other side, many-body interaction due to carrier-carrier and exciton-carrier interactions, which govern the photophysics of 3DP, can also influence the excited state physics of 2DP[16,37,40]. One of the first photophysical analysis has been reported by Zhu’s group aiming to unveil the exciton−exciton interactions in 2DP in the form of $(C_4H_9NH_3I)_2(MAI)_{n-1}(PbI_2)_n$, n = 1, 2, or 3 using femtosecond transient absorption spectroscopy (TAS) [37]. TAS map as a function of pump probe delay and probe wavelength as well as TAS spectra at selected probe wavelengths are

reported in Figure 2d-f. In the first picosecond time scale for *n=1* 2DP, a derivative like feature appears, assigned to a pure blue-shift at the excitonic resonance with no population bleaching at the excitonic resonance (Figure 2d, f). This feature is simulated by the graph in Figure 2e showing the TA signal retrieved from the change in the sample transmittance (or absorbance) before and after the pump pulse. As shown in the picture, a derivative like signal can originate from a rigid blue-shift of the band edge. In this case, similarly to the many-body interactions happening in conventional inorganic QWs, the blue shift can be assigned to band gap renormalization and exciton screening due to multi-particle excitons and exciton-charge interactions. The screening decreases the exciton binding energy leading to the blue-shift of the exciton resonance[40–42]. Notably, this has been shown to be independent from the excitation density and assigned to exciton localization in the disordered energy framework. Note also that a broad weak photobleaching band (i.e. a pump-induced transparency in the sample) is observed below the band gap which originates from filling the trap states lying within the gap as depicted in the cartoon in Figure 2b. If in n=1 the photophysics is mainly dictated by excitons dynamics, what is the main dynamical picture and which are the photoinduced species in n>1 2DP is the next question. It is worth saying that the photophysical processes in n>1 2DP are rather complex, mainly due to the complexity in the fabrication of 2DP with pure phases (especially for n>3), leading to a complicated photophysical scenario. Very limited literature exists so far showing the photophysical processes regulating the n>1 (or quasi-2D). At one side, for n = 2 and 3, a broadening and bleaching of the excitonic resonance have been also observed, in addition to the explained blue-shift. This feature in the TAS gives evidence for the many body interactions due to free carrier formation upon above band gap excitation. A similar behaviour has been well documented for 3DPs, in agreement with the lower exciton binding energy in these materials [37,40]. This suggests that a combination of excitons and charge dynamics govern their photophysics.

2.3. Polaron and Self-trapped exciton Formation

Strong exciton feature in 2DP can also influence the interaction of charge carriers with lattice vibrations (phonons), i.e., the electron phonon coupling[43–46]. This governs the carrier mobilities, modulates the cooling process of hot carriers and dictates the broadening of emission line[43,44]. Interestingly, 2DP have shown in some cases a broad-band emission (Figure 2g, h) that has been assigned to a result of the trapping of the exciton. This phenomenon is known as “self-trapped exciton (STE)” which refers to a bound electron− hole pair that is self-trapped as a small polaron in the lattice distortion field in presence of a strong electron/hole−lattice coupling. Such charge self-trapping is shown to be energetically favoured in 2DP bearing strong excitonic properties and subject to strong distortion of the lead-halide framework. The simplified mechanism for exciton self-trapping is depicted in Figure 2g: upon photoexcitation excitons are formed and can undergo fast relaxation to

self-trapped states with possibly multiple-energy trapped states lying within the material band gap. Thus, the decay from the potential energy surface with multiple local minima results in broad-band emission below the band gap as shown in Figure 2g. The pioneer work showing self-trapped exciton in layered perovskite goes back to 1998 when Ohnishi et al.[47], demonstrated a broad emission line in a 2DP in the form of $(C_2H_5NH_3)_2CdCl_4$ upon varying temperature. They observed a strong exciton-phonon interaction and the subsequent relaxation of the photoexcited free exciton in a STE[47]. More recently, a number of low-dimensional perovskites with different organic cations have also shown broadband emission and the STE emission has been recalled. Few example include the use as organic cations of 3-(aminopropyl)imidazole [47], 2,2'(ethylenedioxy)bis(ethylammonium) (EDBE) and cyclohexyl ammonium cation [46]. In the last case, exploiting the STE concept, white-light emission has been obtained, with a strong potential for white light emitting devices. Notably, the white light emission originates from a distribution of trap states within the gap, upon efficient electron trapping happens due to strong electron-phonon interactions [25].

2.4. Giant Rashba splitting in 2D perovskites.

2D perovskite are an interesting playground for physicists and chemists given their structural tunability driving their physical properties. Among interesting physical phenomena observed, band splitting due to strong spin-orbit coupling (SOC), as first demonstrated by Dresselhaus and Rashba[48,49], has been also observed in 2DP.

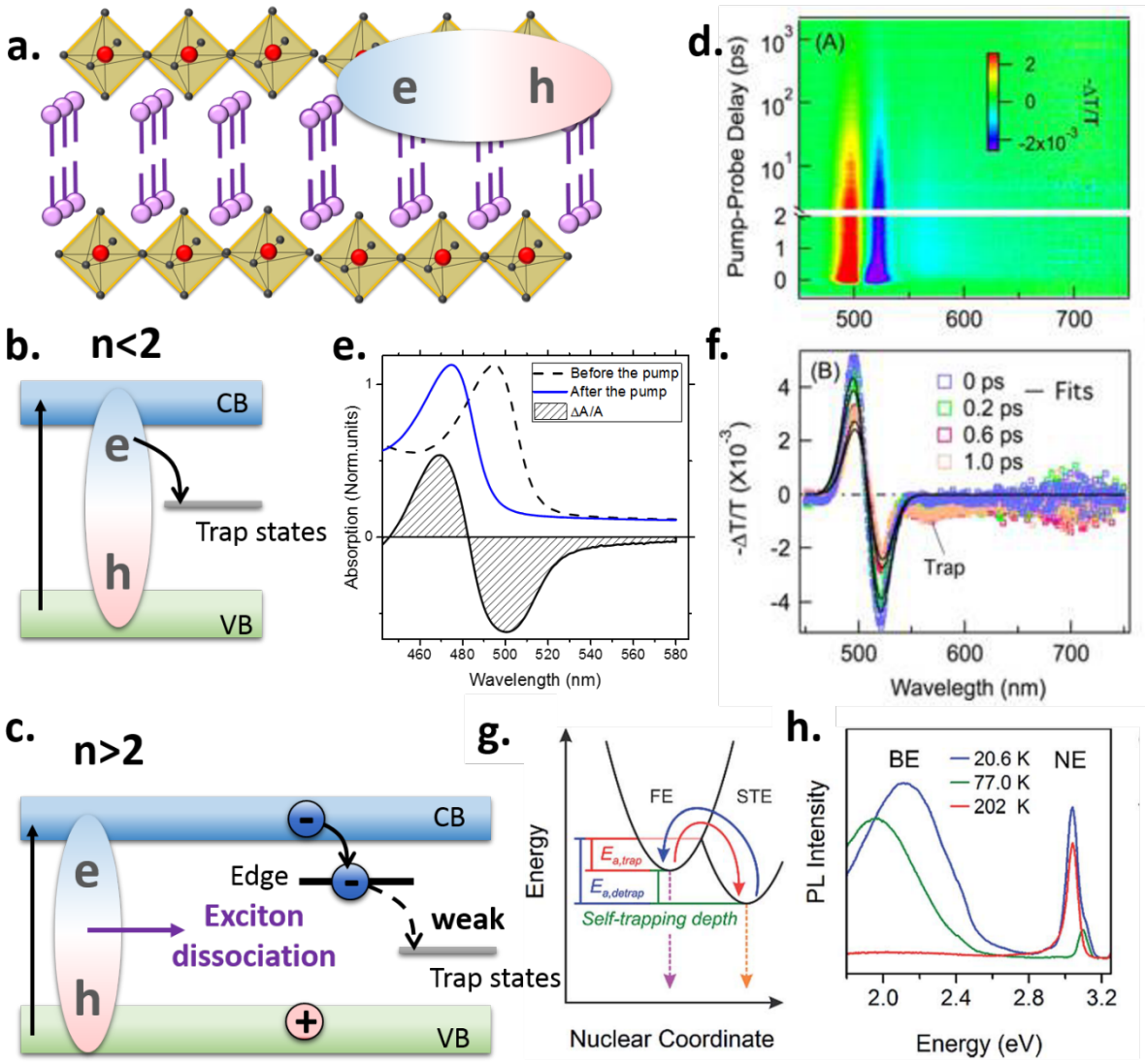

Figure 2. Photophysical processes of 2D perovskite. a. Scheme of the 2D perovskite highlighting the exciton (i.e., electron – hole pair) radius extending on the perovskite. **b.** Scheme of the excited state energy levels in pure 2D perovskite showing the trapping of the exciton for n<2. **c.** Scheme of the excited state energy levels in quasi 2D n>2 showing the exciton dissociation model through the edge states and the weak trapping mechanism. **d.** $\Delta T/T$ (λ, τ) map representing the evolution of the transient absorption signal (TAS) in the picosecond time scale for a pure 2D perovskite and selected traces at different pump-probe delay as shown in panel **f.** Data reproduced from [Wu X. et al J. Phys. Chem. C 2015, 119, 14714]. **e.** Visualization of the TAS showing the derivative spectrum which results from a blue-shift of the absorption edge to the self-normalization of the exciton. **g.** Scheme of the mechanism of exciton self-trapping in 2D perovskite. **h.** Typical Photoluminescence (PL) spectra of a 2D perovskite showing, at low temperature a broad emission band below the gap attributed to the emission from self-trapped excitons.

Considering the electronic properties of the perovskite, the spin-degenerate band dispersion can usually described as a parabolic function in the form of $E(k) = \hbar^2k^2/2m^*$ where m* is the electron effective mass. In the proximity of the band edges, the curvature is thus proportional to the inverse of the m*. The presence of spin-orbit coupling can release the degeneration and even induce a band splitting into two different spin polarized bands (i.e. this happens in the presence of non-centro-symmetric structures with an inversion point of symmetry). In this case the dispersion law can be rewritten as $E\pm(k) = (\hbar 2k2/2m^*) \pm \alpha R|k|$, where αR is defined as Rashba splitting parameter[48].The two Rashba split branches possess opposite spins, which can play a role in the photoexcited state landscape and optoelectronic processes. Zhai et al. have recently applied transient absorption spectroscopy (TAS) combined with theoretical calculations to study the photoexcitations i.e., excitons, and long-lived carriers in a 2DP in the form of $(C_6H_5C_2H_4NH_3)_2PbI_4$ (PEPI)[50] and their dynamical evolution. TAS is indeed a powerful tool to monito the light-activated processes and nature of the excited state species. As mentioned above, in the ultrafast – picosecond- time scale, exicotn bleaching and derivative features are generally observed when probing the visible spectral region. If expanding the spectral extension of the probe light, one could also observe the presence of photoinduced absorption feature which can be assigned to exciton transitions to higher excited states.[50] By measuring the energy of this band, information on first and higher lying excitons as well as biexciton energy levels can be retrieved. In the work from Zhai et al. TAS revealed a photoinduced absorption band in the IR region which has been assigned to an optical transition from the first exciton to a second, upper electron continuum branch. This can only be observable considering that this band comes from a splitting from the lower band by Rashba effect. Comparing the energy of the photoinduced absorption band of the excitonic transitions and the energy of the free carrier absorption one,)a giant Rashba splitting energy has been calculated to be of (40 ± 5) meV with a Rashba parameter of 1.6 ± 0.1 eV·Å. This is due to the inversion symmetry broken in the 2D plane due to displacement of the Pb-I bond, which distorts the overall 2DP structure. [50]. This observation provides an important proof of concept on the possibility to modulate the 2D structure, thanks to the softness of this material, to modulate the structural symmetry. This can trigger the use of 2DP for interesting applications beyond optoelectronics, in the field of spintronics or solar-spintronics which exploit the enhanced spin-to-charge conversion efficiency.

3. Stability as the current issue for 3D Hybrid Perovskites solar cells.

3.1. Stability tests: the need for standardized tests.

Given the high urgency and actual issues on perovskite device stability, it is worth mentioning, before describing the experimental results, how solar cell stability tests are usually performed. In general, a device is considered stable if it shows less than 20% drop of performance at 85° C performance after 1,000 h AM 1.5G illumination (IEC 61646-type test). This condition comes from an equivalence to have a lifetime which compares to 25 years, which is what the market asks for a commercial product. Certainly, there is no meaning that a solar technology will last for 25 years, without having it in the field for 25 years. However, since this is infeasible in the timeframe of product development, and indeed in the timeframe a research work, accelerated testing are usually employed. This corresponds, for instance to aging the solar cells at 85°C under simulated full sun illumination with the target of achieving less than 20% drop in performance after 1000 h illumination. This number comes from considering: 25 years ~ 54,750 h full sun illumination assuming the equivalent of 6h full sun-light/day. Taking a standard acceleration factor of 2 for each ten degrees increase in temperature, an acceleration factor of 2^6=64 is estimated going from 25°C to 85 °C, and hence the 54,750 hrs equivalent would be obtained before 1000 h. Despite the concept, clear *per se*, a huge number of different stability conditions have been set and presented in literature, making a straightforward comparison among them challenging. The large variation on the conditions at which the solar cells are usually tested (i.e. full sunlight illumination or just exposed to random sunlight ambient conditions), and the kind of device tested (encapsulated or not) has been responsible of a large confusion in the literature which still lacks of a uniformed standards. The term "ambient" conditions, for instance, encompasses a broad range of possible cases, such as different relative humidity used. To overcome the stability issue, accelerate the understanding and ensure the progress in the field, comparable tests are necessary. For instance, in the community of organic solar cells, the International Summit on Organic Solar Cells Stability (ISOS) has been established to have a defined internationally valid protocols that can compare lab to industrial results.) A direct translation of this standard to perovskite solar cells is rather challenging given additional parameters which affect the device stability and operation, such as the hysteresis in the J- V characteristics. In the review, given the variety of measurements conditions, we reported the one used in each measurements reported.

3.2. Stability issue in 3D Hybrid Perovskites.

The boom in the perovskite materials and devices is confronted with severe stability issues, which are incompatible with the current PV market requirements (e.g., 0.25 to 0.5% losses per year)[5]. Device degradation is due to both intrinsic and extrinsic mechanisms[6]. In presence of water, 3DP reacts leading to the collapse of the structure either forming a 0-dimensional hydrated phase or undergoing irreversible decomposition back into the precursors (Figure 3a). $CH_3NH_3PbI_3$, for instance, starts to decompose at a humidity of 55%, inducing a remarkable bleach of the colour that changes from dark

brown to yellow due to conversion into PbI_2 (Figure 1d)[6,18]. On the other side, photo-induced oxygen degradation can also lead to the generation of superoxide species (Figure 3b). This reactive O_2 species can deprotonate the methylammonium cation (CH_3NH_3) of photo-excited $CH_3NH_3PbI_3$*, triggering the decomposition back into the precursors[51]. Oxygen can diffuse in the intergranular regions and permeate in the perovskite bulk. As a result, superoxide can form at the perovskite crystal grain borders triggering a surface reaction. Thereafter, oxygen diffuses occupying the bulk iodide vacancies while being reduced, leading to full structural degradation of the material (see Figure 3b). Local heating and UV light also accelerate perovskite decomposition.[6,18] Other phenomena such as light induced ion movement, "photo-instability", or structural deformations do not only disturb the material stability, but also alter the device behaviour, contributing to the anomalous hysteresis behaviour observed in the current-voltage characteristics of device that has not yet been clearly understood.[52–55] It is fair noticing that, while the degradation factors such as moisture, oxygen, and heat can be circumvented by controlled encapsulation processes, instability upon light illumination is inevitable for 3D mixed halide perovskites. Light soaking even in an inert atmosphere can also trigger the device degradation. At one side, illumination induces halide segregation into iodide-rich and bromide-rich domains resulting in a variation of the material's optical/electrical response and dynamical behavior, reversible only up to a certain extent. At the other, laser irradiation has been demonstrated to cause partial decomposition of MAPbI3 surface forming a new metallic Pb component, which achieves a saturation level after hundreds hours of continuous illumination. In addition, the chemical and electronic structure of the perovskite might also be affected by white light illumination leading to the formation of PbI2 defects. In particular, it has been shown that degradations starts at perovskite grain boundaries: here defects can create additional photoinduced electronic traps which would perturb the crystal system and induce lattice distortion until the eventual degradation of the perovskite structure. More in details, light can break the C−N bonds in the organic MA into hydrocarbons and ammonia gas, leaving residuals of PbI_2X (X=halogen), or metallic Pb in the film. It is also worth mentioning that UV part of white light can be detrimental for the perovskite device behavior. In particular, this is due to the sensitivity of the TiO_2 layer susceptible to UV-induced degradation. Rapid deterioration resulted from electrons injected intoTiO2 becoming trapped in deeply unoccupied sites. To this regard, functionalization of the TiO2 surface traps, suing for instance 2D perovskite with carboxylic acid ending group can be a promising strategy, as shown in [].

3.3. Strategies to overcome stability issues in 3D perovskites.

Despite the urgency, only in the last couple of years a significant attention has been devoted to face the stability issue[1,3,5,20,56]. The stability issue can be evaluate from two complementary perspectives,

considering the intrinsic stability of the bulk material or the extrinsic stability of the device, the latest resulting from considering the whole device structure and interfaces (such as the top organic HTM). From a material point of view, different routes have been proposed. Crystal engineering, i.e. the exploration of a mixture of alternative cations, for instance, has been a viable solution towards the stabilization of 3DP structure. Examples include the introduction of Cs^+ and Rb^+ into the hybrid $(FAPbI_3)_{0.85}(MAPbBr_3)_{0.15}$, leading to a complex triple[15] and quadruple[16] cation cascade which stabilize the 3D structure, limiting the light-induced ion dispersion in the bulk. This resulted in devices with PCE over 20% and reasonably good long-term stability (Figure 3c). Their incorporation alter or eliminate unwanted crystal phases and control of the crystal quality[54,57,58,59], i.e., reducing defect densities at grain boundaries. However, given the limited choice of the organic cation and the experimental difficulties in obtaining good perovskite films with mixed cations, this strategy is still challenging and subject of ongoing research. Despite the strict limit imposed by the Goldschmidt law, as reviewed in Section 1., we have recently demonstrated that the incorporation of relatively large organic cation, theGuanidinium (Gua), into the $MAPbI_3$ crystal structure can improve the material stability (Figure 3e)[60]. *Per se*, Gua-based perovskites arrange into a low dimensional perovskite phase [61]. However, when added in a small amount (up to a maximum 25%) in the $MAPbI_3$, it inserts in the 3DP network.. This slightly deforms the crystal lattice, but, on the same time, improves the structural stability thanks to the increased organic-inorganic interaction through the additional hydrogen bonds formed with the inorganic cage (Gua forms six hydrogen bonding with iodine, ultimately reducing the H—I distance). $Gua_{0.14}MA_{0.86}PbI_3$ delivers in solar cells an average PCE over 19%, and stabilized performance for 1000 h measured at around 60 °C maintained at the maximum power point under argon atmosphere and under continuous light illumination (Figure 3d)[60]. From the second point of view, each interface and contact layer of the device stack plays an important role in the overall stability. Upon proper interface modification, degradation can be suppressed.Examples include the use of thin layers of Al_2O_3, NiO barrier or the incorporation of luminescent photopolymers.[19,20] For instance, Guarnera et al. attempted to enhance the device stability by incorporating a buffer layer of Al_2O_3 nanoparticles, between the perovskite and the top HTM. Devices were encapsulated in nitrogen conditions using an epoxy resin. While the devices without the buffer oxide layers experienced degradation upon 200 hours, devices with the buffer layer show better resilience. This was suggested to be related to a blocking effect of the buffer layer in contrasting the migration of metals from the perovskite surface to the HTM. At the same time, electron transport and hole transport materials (ETM and HTM, respectively)—which serve as charge-selective extraction layers—and the metal electrodes used in the devices are critical to device stability. The commonly used molecular HTM, i.e. Spiro-OMeTAD, contains lithium bis(trifluoromethylsulfonyl)imide (LiTFSI) used as a *p*-dopant to enhance the

conductivity and hole mobility. However, the hygroscopic Li^+ cations are highly mobile and can migrate throughout the device stack during the operation, which results in the unintentional modification of the active layer, which can initiate a crystallization under thermal stress which might open then the gate for the diffusion of the top metal contact into the perovskite[62]. This represents an additional external factor for device degradation which has been taken in consideration. Alternative electrodes can alleviate this issue as for example the use of polymeric layer, PTAA[12], or carbon based electrodes[11,63]. This configuration, known as carbon-based or monolithic solar cells, has recently attracted a lot of interest for the superior stability as described more in details in Section 4.2. One strategy includes the replacement of the organic HTM, such as the commonly used spiro-OMeTAD with Li^+-free hydrophobic HTM. Examples includes 9-(2-ethylhexyl)-*N*,*N*,*N*,*N*-tetrakis(4-methoxyphenyl)-9H-carbazole-2,7-diamine polymers used to replace Spiro-OMeTAD, which resulted in enhanced stability, retaining 95% of the PCE for 1500 hours under inert atmosphere testing, at the expense, however, of the device efficiency, of around 16%. On the other side, the use of inorganic HTM, such as combining copper(I) thiocyanate (CuSCN) and reduced graphene oxide, has increased the device stability while showing 20% PCE. CuSCN combines high mobility and good thermal stability which resulted in solar cells with prolonged stability for 1,000 h examined at a maximum power point under continuous full-sun illumination at 60°C in a nitrogen atmosphere (see figure 3e). On the other side, mesoporous TiO2 ETM can affect the stability upon UV irradiation, due to UV-induced photocatalysis. In the search for TiO_2 alternatives, Lanthanum (La)–doped $BaSnO_3$ (LBSO) perovskite nanoparticles have been recently implemented as a valid solution for their promising characteristics in terms of wide band gap, high electron mobility and inferior UV photocatalytic ability. Using this doubled inorganic/hybrid perovskite stack, efficiency beyond 21% has been reached. Remarkably high photostability under light illumination, including UV has been demonstrated (see Figure 3f, g): the LBSO cell retained 93.3% of its initial performance after 1000 hours, whereas the TiO2 cell completely degraded within 500 hours (measured under full sun illumination, encapsulated devices).

To conclude, it is also worth mentioning that a big role in limit the adventitious infiltration of water in perovskite solar cells is played by use of easy encapsulation strategies, especially in view of the near future commercialization. In general, tests using encapsulated devices use easy and rudimentary methods to encapsulate small area devices. Typically, the device is covered by a thin glass cover slip, which is sealed using a UV curable epoxy resin filled between the metal contact and the glass coverlid. On the other side, complete know-how on device encapsulation exists in the display technology. In this case, the glass placed on top of the electrode leaves a gap which is filled by a dessicant able to adsorb water which could have penetrated through the epoxy resin. Despite advantageous, these manual encapsulation techniques would not be ideal for upscale mass-production.

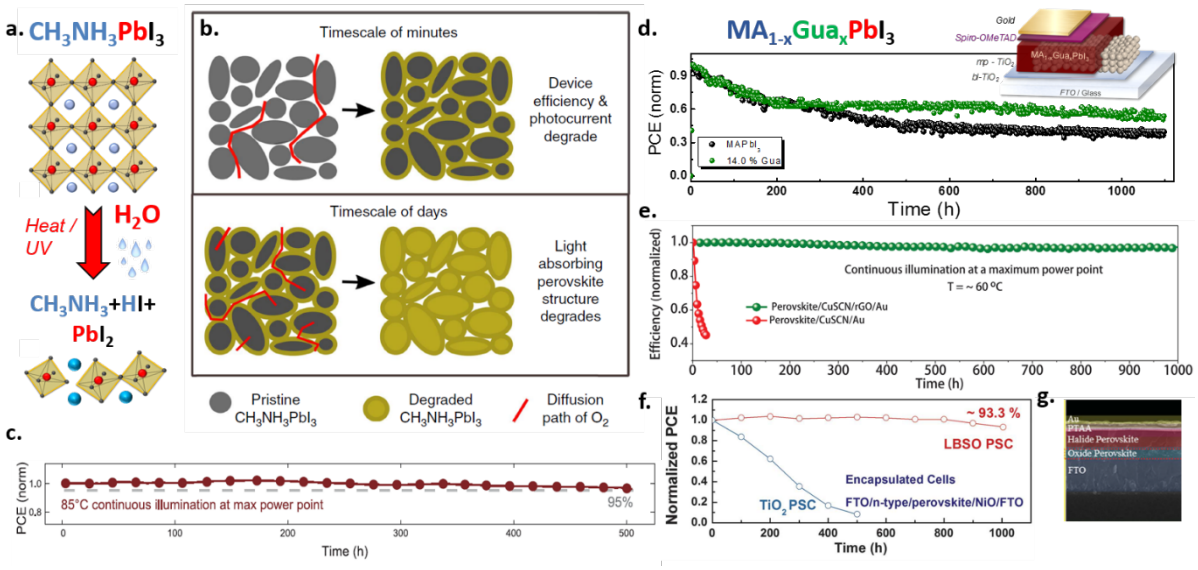

Figure 3. Degradation of 3D perovskite and latest improvement in the 3D perovskite solar cells stability. a. Scheme of the degradation of the 3D perovskite material. Upon exposure to Water, oxygen the material decomposes back to the precursors. **b.** Degradation processes initiated by infiltration of oxygen through the perovskite grains. Data reproduced from [Aristidou N. et al Nature Communications volume 8, Article number: 15218 (2017)]. **c.** Power conversion Efficiency (PCE) versus time, indicating the perovskite solar cell stability measured under accelerated tests. Data retrieved from [Saliba M. et al *Science* 354, 206 (2016)]. **d.** solar cell stability data using a combination of cations in the form of $MA_{1-x}Gua_xPbI_3$ developed in our group. **e.** solar cell stability using CuSCN and rGO replacing the organic HTM. Data from [Arora et al., *Science* 358, 768–771 (2017)]. **f.** Solar cell stability data using . Lanthanum (La)–doped BaSnO3 (LBSO) perovskite as electron transport layer. As sketched in the cross-sectional Scanning Electron Image in panel **g.** Data from [Shin et al., *Science* 356, 167–171 (2017)].

In particular, using this architecture along with a mixture of 2D and 3DP (as we will present more in detail in Section 4), in 2017, we have obtained record PSC lifetime of more than 1 year at PCE=12%[11]. This is a remarkable result, although the PCE is still lower compared to the best perovskite solar cells to date.

In the following we describe in details a new perspective to solve the stability issue by exploiting the superior stability character of the 2DP. Notably, the higher resistance to moisture is mainly due to the hydrophobic nature of the **R** cation, as well as the highly oriented structure and dense packing into which the 2DP self-organizes[8,10]. This in turns reduces the grain boundaries and prevents direct contact of adventitious water with the perovskite, ultimately boosting the stability. Note that 2DPs, despite being tunable, are usually not optimal for solar cell application if n<2, while they can be interesting light antennas if n>2[22]. However, if combined together with 3DP in a 2D/3D hybrid, a synergic action

can be designed to boost efficiency and stability. In the next section, we will review the main device configurations and results reported so far embodying quasi-2D as well as 2D/3D hybrid active layers.

4. Stable Perovskites solar cells with 2D Perovskite.

4.1. From Quasi-2D to 3D Perovskites Devices: Design, Efficiency and Stability

Phenethylamine (PEA) and butylamine (BA) based quasi-2DP have been pioneer candidates as active layers in 2DP solar cells. Using $PEA_2MA_2Pb_3I_{10}$, initial PCE of 4.73% have been demonstrated[13]. Importantly, the thin films do not show any sign of degradation upon 2 months exposure under a 40% humidity condition, , showing a remarkable moisture resistance. $BA_2MA_{n-1}PbI_{3n+1}$ (n=1- 4) also show similar PCE, which remain stable in humid environment for about two months[22]. These seminal works have opened the way for a massive interest in the use of quasi-2DP for stable solar cells. The bulky cation can impart hydrophobicity to the perovskite, improving their resilience to moisture and humidity (see the pictures in Figure 1 showing the retarded degradation upon exposure to humidity for 2DP)[8,9,22]. However, solar cell performance is relatively poor. This is mainly ascribed to the narrower absorption of the 2D perovskite, stronger exciton binding energy, and inhibited charge transport across the organic planes as discussed in Section 2.1. The latest in particular, is strongly affected by the morphology and deposition of the 2D layers. The 2D perovskites self-assemble to form uniform film with perfect surface coverage and a homogeneous texture. This is induced by the 2D nature of the material, which spontaneously forms highly oriented crystals with only a few grain boundaries. Interestingly, such uniform 2D films are promptly formed immediately after the spin coating, without the need of annealing, as for the 3D. Usually, the 2DP grows with an orientation parallel to the substrate, especially for n=1, as a result from the in plane growth induced by the layered structure[8]. As a consequence, the charge transport is good along the metal halide lattices, whereas it gets hindered in the perpendicular directions (across the interlayers, in the organic barriers). This has been a common drawback for single-step deposited 2D perovskite solar cells, as reviewed in the Section 2.1, resulting in a relatively low fi ll factor (FF) and photocurrent. The use of multiple cations or different strategies to impart the optimal crystallizing direction of 2D perovskites represent a promising route to enhance charge transport and extraction, to deliver high device efficiency along with improved material stability. For instance, for n>1, adding MA in the organic composition, a competition arises between the BA ions, which try to confine the growth within the planar layer, and the MA ions, which try to expand the perovskite growth outside the layer. In this case a vertical growth of the compound with respect to the substrate plane is observed, which is beneficial for vertical charge transport.[22]

Vast research on optimizing the solution-processing methods is still ongoing in order to define a way to control the crystal growth to impart directional charge transport which happens along the inorganic backbone. For instance, different deposition processes have been tested, including the hot-casting (HC) method, to obtain high-quality 2DP film with a remarkable preferential cross-plane alignment, in order to facilitate efficient charge transport. In this way, PCE up to 12.52% have been obtained, with no hysteresis, and greatly improved stability in comparison to 3DP when exposed to light, humidity and heat stress tests[9]. More in details, to perform a quantitative analysis, they use a different model to evaluate the stability by fitting the post `burn-in' section of the PCE to a straight line and extrapolate the curve back to zero time to obtain the PCE at time=0. Lifetime is then derived from t=0 to the time at which the device shows 80% degradation, surpassing of 1,000 h stability for an unsealed perovskite cell and reaching 4,000h for the encapsulated device. In a way to impart a preferential orientation to the growth of the 2DP, crucial for the transport and device performances, different strategies have been further explored[64]. A different example used a slightly modified BA cation, namely *iso-BA,* containing short branched-chain spacer cations and showing a remarkable increase in the crystallinity compared to the standard *n*-$BA_2(MA)_3Pb_4I_{13}$. In this case, the out-of-plane crystal orientation of *iso*-$BA_2(MA)_3Pb_4I_{13}$ film notably increases, which dramatically enhance the charge transport and extraction. Using *iso*-$BA_2(MA)_3Pb_4I_{13}$ in an inverted configuration between C_{60} and spiro-OMeTAD PCE= 8.82% have been obtained, three times higher than that of the *n*-$BA_2(MA)_3Pb_4I_{13}$ counterpart[65]. Moreover, upon applying the HC technique, a PCE= 10.63% has been reached. Remarkably, the *iso*-$BA_2(MA)_3Pb_4I_{13}$ perovskites film exhibit high ambient stability even without encapsulation[65] for 800 hours storing the sample in an environmental chamber at 20 °C with a high relative humidity (RH) of 60%. On the other side, Cs-doping has been used to enhance the crystal quality. This resulted also in a reduced trap-state density, enhanced charge-carrier mobility and charge-transfer kinetics. PCE of 13.7% and excellent stability (measured under constant illumination at 40-50 relative humidity) have been demonstrated[66]. Different 2DP have been also developed by incorporating more complex cations, such as $(EDA)(MA)_2Pb_3I_{10}$ (EDA = ethylenediamine). Thanks to the doubled hydrogen bonding to the inorganic layer, the crystal quality was enhanced. This improved the material stability of solar cells tested in an ambient environment after encapsulation using UV-epoxy, delivering PCE=11.58%[67]. Very recently, it has been shown that it has been able to control the vertical growth of 2DP, in the form of $BA_2MA_3Pb_4I_{13}$ resulting in drastically enhanced PCE with respect to the randomly oriented 2D film. This has been obtained upon understanding and controlling the nucleation and growth of 2DP at the liquid–air interface. At this interface, a top-crust with strong vertical orientation is formed which can then tune the 2DP orientation. The authors suggest that the butylammonium molecules are bounded to the lead iodide slabs in such a way that the butyl chain are pointing toward outside,

inducing the vertical orientation of the 2DP (see Figure 4f XXXXXXXXX). This has been obtained through a "pre-crystallization annealing" step where the BA2MA3Pb4I13 film crystallizes on a hotplate at elevated temperature with minimal spin-induced convection and without being exposed to temperature for prolonged time. After the crystallization has been completed during the spinning, a thermal gradient is applied. The pre-crystallization annealed film with a strong vertical orientation outperforms the films with partial random orientation due to a significantly higher short circuit current density, delivering a PCE=9.7%. However, no results on the device stability have been commented, casting the doubt of the stability versus efficiency relationship, still far to be elucidated. Using a similar 2DP, (in the form of $BA_2MA_3Pb_4I_{13}$), PCE as high as 11% has been obtained. The results comes from a careful control on the 2D thickness of around 200nm, the optimal compromise between photogeneration of carriers (absorption) and carrier transport through the layer thickness.

Besides tailoring the organic cations, varying *n* towards high value has been demonstrated as a valid approach to boost device efficiency[22]. It is fair to highlight, however, that despite the modest efficiency used (see graph in Figure 4a), especially for n>3 2DP, a trade-off exists between efficiency and stability, in relation to the number of layers' n of the quasi-2DP. As shown in Figure 4b and c, n=1 solar cells delivers the best stability, at the expense, however, of device PCE. On the other side, increasing n, performances boost and stability decreases. Phenylethylammonium (PEA) based quasi-2DP have been realized in the form of $PEA_2(MA)_{n-1}Pb_nBr_{3n+1}$ (n=40, 50, 60) tuning their dimensionality from *n=1* to n>60. For n=60 a certified PCE=15.3% has been shown in inverted device configuration, keeping a good device longevity for 60 days under a low humidity atmosphere [22,27,29]. Importantly, in analogous studies under humid air (55% RH), while the 3DP looses 80% of the initial performances in 3 days, 2DP could resist for over 2 weeks under high RH (for n = 60 and n = 40 devices).[27]

Similarly, they have been also employed in mesoporous based solar cells[7,68,69]. A high V_{OC} of 1.3 V or 1.46 V was obtained with/out the organic HTM showing a PCEs of 6.3% and 8.5%, respectively[69]. However, if *n* becomes too large, the formation of 2DP domains is limited, reducing device stability measured in this case at 90°C at 50% RH. In addition to the common monoammonium cation like BA and PEA, multiammonium cations containing polyethyleneimine (PEI) cations forming $PEI_2MA_{n-1}Pb_nI_{3n+1}$ (n= 3, 4, 5, and 7) have also been incorporated in 2DP solar cells. The use of intercalated PEI improved the flow of charge and their transport leading to PCE=8.77% under ambient humidity (tested under ambient conditions with a humidity of approximately 50%, without encapsulation.)[70,71]. Increasing n, solar cells using $PEI_2MA_6Pb_7I_{22}$ and $PEI_2MA_4Pb_5I_{16}$ show much improved stability even without sealing, with PCE around 15%. Other examples reported the use of $(IC_2H_4NH_3)_2MA_{n-1}Pb_nI_{3n+1}$ deposited through a sequential deposition method under ambient conditions in which the dimensionality of perovskite is controlled by the dipping duration[72]. As a result, the increased *n* ,

corresponding to the enlarged stacking of the closely packed metal halide layers and a resultant smaller band gap, offers broader absorption and higher photocurrent. As a result, a maximum PCE=9% has been achieved with remarkably good stability (they compared fresh devices and aged ones upon four days after the fabrication. The devices were stored under ambient condition (25 °C, 70%–80% RH) without any encapsulation).

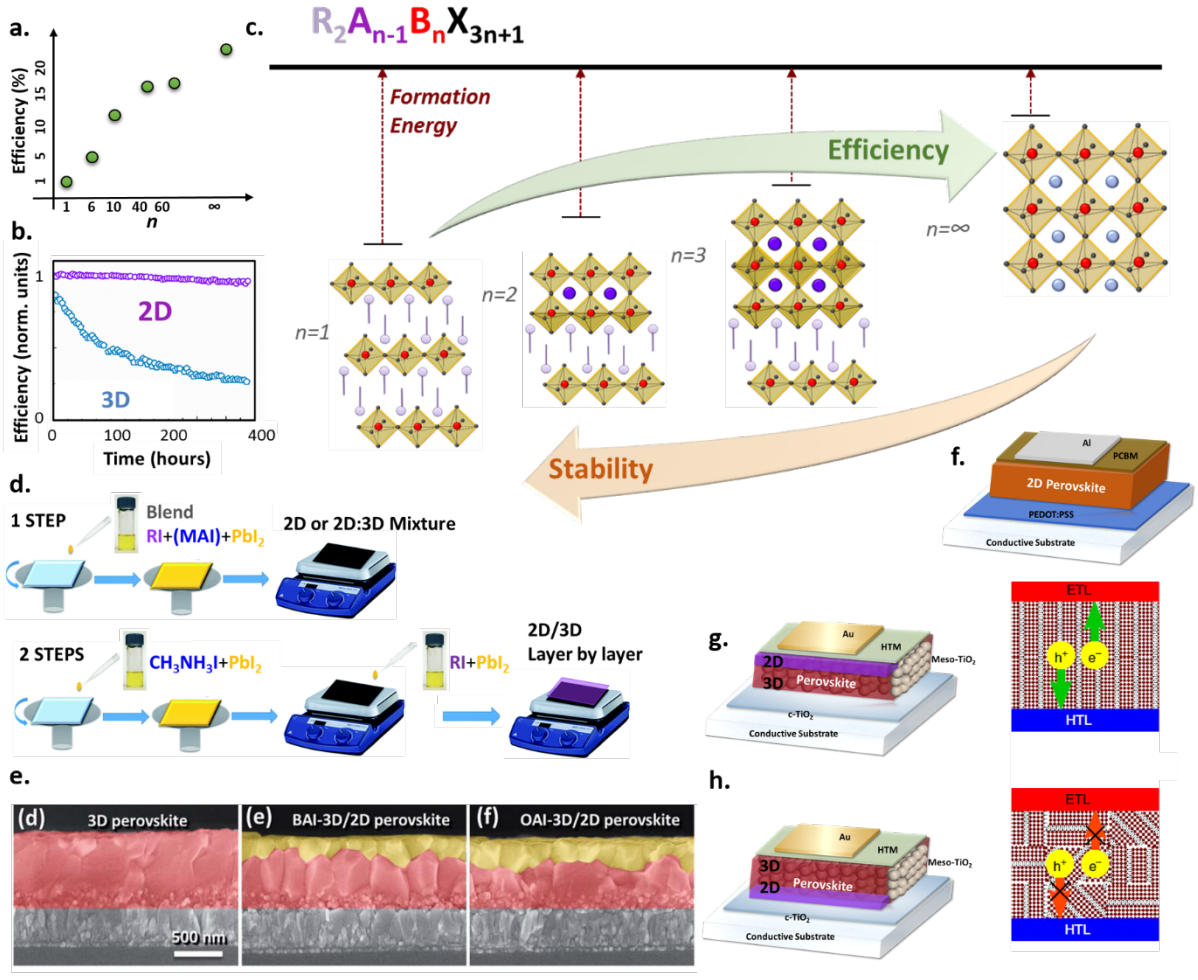

Figure 4. 2D perovskite based solar cells: processing and device structures. a. Graph reporting the PCE versus n (number of layers in the quasi-2D perovskites); n=∞ corresponds to the 3D perovskite. **b.** Comparison of stability data (showing PCE versus time) for two standard perovskite solar cells developed in our lab comparing 2D versus 3D perovskites. **c.** cartoon of 2D – quasi 2D – 3D perovskite showing the reduced formation energy going from 2D to 3D as well as the increased efficiency, at the expense of a reduced stability. **d.** Schemes of the depositions methods used so far for the processing of 2D or 2D:3D mixture perovskites based on 1 step approach or 2 step one to obtain a layer by layer 2D/3D. **e.** cross-sectional Scanning Electron Microscope Images comparing the 3D film with different 3D/2D layer by layer films. Data retrieved from [J. Mater. Chem. A, 2018,

6, 2122]. **f. – h.** scheme of the solar cells device architectures employed so far in literature using either a pure 2D (**f.**) – in this case optimal vertical alignment of the inorganic chain is desiderable to ensure charge transport to the top and bottom electrode - or a bilayer structure where the 2D is deposited on top of the 3D (**g.**) or on the bottom layer (**h.**).

4.2. Combining perovskite with different dimensionality for solar cells into a 2D/3D mixture

A different concept has been put forward combining the low dimensional perovskite together with standard 3D into a hybrid 2D/3D composite. The idea is to join in a synergistic approach the high efficiency of the 3D with the superior stability of the 2D, while keeping the structural integrity of the two phases. 2DP acts as a protective barrier against humidity while preserving efficient charge transfer flow in the hybrid system. Following this strategy, we developed a 2D/3D composite mixing $MAPbI_3$ with a 2DP in the form $(HOOC(CH_2)_4NH_3)_2$ (i.e. ammonium valeric acid, AVA) through a simple 1 step deposition approach by blending the precursors solutions (see Figure 4d)[11]. The presence of the COOH ending group in the AVA cation leads to a favourable anchoring to the mesoporous TiO_2 layer forming a thin 2D layer at the oxide surface. This induces a vertical graded structure where the 2D templates the growth of a highly oriented 3DP on top forming a 2D / 3D layered system. This layered 2D/3D architectures has been implemented in both standard mesoporous TiO2/SpiroOMeTAD solar cells as well as in monolithic solar cell where the HTM and Gold are replaced by Carbon layer. This represents an extremely interesting configuration due to the lower cost of carbon and enhanced resistivity to water permeation, which makes it intrinsically a more stable solution. In both cases enhanced stability has been obtained. This has been ascribed to the enhanced structural stability of the 2D/3D layers as well as a possible passivation of the TiO2 surface through the 2D perovskite bonds. In particular, for the case of monolithic devices (fabricated either on lab scale and on 10x10 cm^2 large module) the use of 2D/3D impart enhanced stability, for 10,000 h with no losses in performances. (tests performed at 55°C, 1sun illumination for 24 h per day, sealed under ambient atmosphere with glass slide and Surlyn polymer. An ultraviolet filter up to 390nm was used on top of all over the samples. Solar simulator class A 1.5M at full sun under short circuit condition). This lead to a world record-stability of more than 1 year, as indicated in Figure 5a. Although the efficiency is still moderate, this work has triggered much interest also on the industrial scale, showing the potential for a scale-up of perovskite technology.

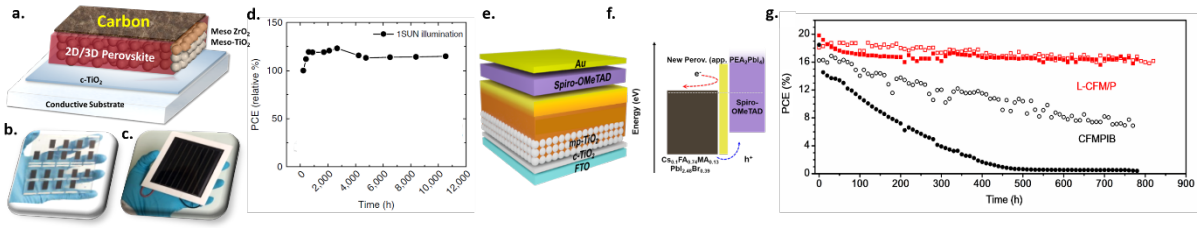

Figure 5. Record- stability for 2D/3D mixed perovskite solar cells. a. – d. Recent results reporting the use of a 2D/3D composite for highly stable devices perovskite devices. a. Device cartoon of the Hole transporting Material (HTM)-free solar cell and of the standard HTM-based solar cell. **b., c.** Pictures of the lab cells and photovoltaic large module developed, respectively. **d.** Typical module stability test Data retrieved from [G. Grancini et al. Nature Comm. 8, 15684 (2017)]. **e.** scheme of the solar cell architecture of a 3D/2D layer by layer solar cell using PEAI to form the 2D layer and **f.** relative energy level alignment scheme. **g.** 3D/2D device stability (**h.**) Data reproduced from [Cho K.-T et al Energy Environ. Sci., DOI: 10.1039/C7EE03513F (2018)].

A number of work have been demonstrating the benefits from combining 2D and 3D perovskites together. 2D/3D junction have been employed in both mesoporous solar cell (see device cartoon in Figure 4 f-h) as well as in inverted architecture using PEDOT:PSS and PCBM as selective extraction layers[12,64,66,73,74]. Both one step and a sequential 2 step methods have been optimized to deposit the 3D/2D bilayer. For instance, Ma et al.[73], use a two-step method for the deposition of $MAPbI_xCl_{3-x}$ treated with cyclopropylammonium iodide (CAI). This precursor, reacting with the excess of PbI_2 present in the 3D, induces the formation of the 2D CA_2PbI_4 perovskite on top (Figure 4d). Such 3D/2D-based solar cell delivers PCE=13% stable for 40 days (devices were stored and tested without encapsulation. Devices were exposed directly to the environment without any cover, in an ambient environment at room temperature with 63 ± 5% humidity), outperforming the 3D device. 3D/2D bilayer made of $MAPbX_3$ and PEI_2PbI_4 formed in situ on top of the 3DP have been also realized[70]. The moisture-resistant 2DP top layer induces the growth of a high-quality 3D on top, ultimately enhancing the long-term stability of the cell stack. Remarkably, a maximum PCE=13.8% has been achieved on a flexible substrate. With a similar approach, an ultrathin 2DP $(5\text{-AVA})_2PbI_4$ (5-AVA=5-ammoniumvaleric acid), on top of $(FAPbI_3)_{0.88}(CsPbBr_3)_{0.12}$ has been engineered[75]. This enhances the moisture- and photo-stability as compared to the control perovskite film due to hydrophobic nature of 2DP. PCE is boosted from 13.72 (only 3D) to 16.75% (2D/3D). Interestingly, hysteresis is found to be reduced by the 2DP layer. This is assigned to an enhanced interfacial charge extraction and reduced recombination. Overall, despite the promising results in terms of device longevity, PCEs reported so far span over a range from 13 to 17%. Importantly, devices show less than 10% drop in performances considering different conditions from 10% RH, to 40% and 80% as well as upon exposure to thermal

stress (one cycle: heating at 85 ° C for 2 h and room temperature for 1 h). Despite the important improvement in the field, the challenge is still to obtain a high efficient and stable (as defined by the standards) solar cells. Aiming to reach the goal and approach the 22% efficiency of 3D PSC, we recently developed a controlled layer by layer growth of PEAI- based on top of a mixed $Cs_{0.1}FA_{0.74}MA_{0.13}PbI_{2.48}Br_{0.39}$[12]. The device architecture and interface energy level alignment are depicted in Figure 5 e, f. The layer by layer growth is induced by dynamically spin coating the PEAI in isopropanol (IPA) solution on an optimized mixed perovskite with excess PbI_2. Given that the excess of PbI_2 segregates on the top of the 3DP (see carton in Figure 5e), the added PEAI reacts in situ with the PbI_2 forming the 2D only on the top surface. Being at the top surface, and then at the interface with the HTM, the interfacial charge carrier recombination is reduced, and the efficiency enhanced over 20%. PSCs retain 85% of their initial PCE stressed under one sun illumination for 800 hours at 50°C in an ambient environment, showing the first example of high efficient and stable 2D/3D device (see Figure 5 g, h). Importantly, this result sets the first step in the community which demonstrate enhanced stability without compromising the PCE, but reaching efficiency comparable to the ones of 3D PSCs.

4.3. 2D as dopant to passivate traps at the 3D grain boundaries.

A blend of 2D and 3D has been also employed with the idea to use the 2D as a dopant agent to passivate the 3DP traps at grain boundaries[74]. This concept is schematically depicted in Figure 6a. For example, mixed- $FA_xPEA_{1-x}PbI_3$ have been developed with this intent. PEA cation infiltrates in the grain boundaries while keeping the 3D structure. It also serves as linking additive to tighten the $FAPbI_3$ crystal domains and improve the film crystallinity. Inverted devices using NiOx and PCBM selective contacts demonstrate a PCE of 17.7%. Another example used PEA_2PbI_4 to dope $MAPbI_3$ forming a mixed $(PEA_2PbI_4)_{0.017}(MAPbI_3)$. As a result of grain boundaries passivation, ion migration is blocked[76]. High PCE of 19.8% are obtained stable for over 40 days without encapsulation at 60–90% relative humidity at room temperature. In a similar fashion, 10% of PEA^+ has been mixed into $(FAPbI_3)_{0.85}(MAPbBr_3)_{0.15}$ perovskite to passivate the grain boundaries while also acting at interfacial layer on top of the TiO_2[77]. This results in improved device open-circuit voltages (V_{OC}) reaching a maximum PCE= 17.1% and better stability (for more than 1,000 hours during upon exposure to RH = 70% in the dark). Given that degradation of perovskite films is initiated from the defects sites not only at grain boundaries, but also at the surface, 2DP can also function as a protective shell. For instance, a 2D/3D interface has been engineered by inducing the reaction of n-BA with the surface of 3DP, producing a $(BA)_2PbI_4$ surface layer, as shown by the cross sectional scanning electron microscopy image in Figure 4e. At the surface, trap-assisted recombination is reduced, as well as trap state densities, as a result of the defect passivation[78]. As an effect, carrier lifetime is extended, ultimately

leading to increased PCE to 19.56%. Device PCE is retained for more than 85% for 100h considering unsealed mesoporous devices which were stored under 50% relative humidity and dark conditions. To further push this concept, more complex 2D/3D perovskite interfaces have been designed "ad hoc" to form a hybrid system with alternating 2D and 3D phases (see Figure 6b). The 2DP can, for instance, aggregate in platelets which are interspersed between the highly oriented 3DP grains forming a 2D/3D/2D/3D interfaces. As shown in Figure 6b, this approach leads to reduced non-radiative charge recombination. More in details, this can be realized using n-BA cations into a mixed-3DP in the form of $FA_{0.83}Cs_{0.17}Pb(I_yBr_{1=y})_3$[64]. A stabilized PCE of 17.5% has been obtained stable for 1000 h, as described earlier in this review.

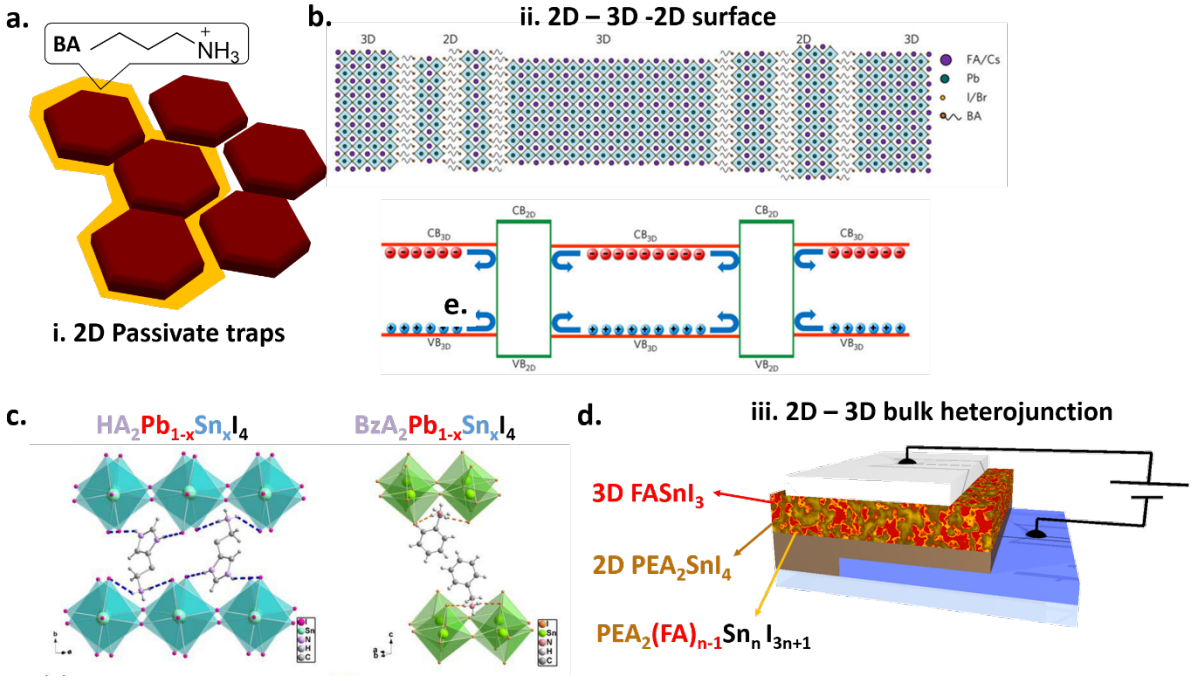

Figure 6. Integration of 2D perovskite into 3D for stable perovskite solar cells. a. Scheme of the use of 2D perovskite as dopant agent to passivate the crystal grain boundaries of 3D perovskite. **b.** Formation of a 3D/2D/3D structure for efficient and stable solar cell. Data reproduced from [Wang Z. et al. Nature Energy 2, 17135 (2017)]. **c.** Sn-based 2D perovskites. Data reproduced from [Mao L. et al. Chem. Mater. 28, 7781 (2016). **d.** Cartoon of 2D – 3D perovskite (Sn –based) mixed together resembling a bulk –heterojunction morphology.

4.4. Emerging Lead free- Sn based 2D perovskites

Research towards alternative to lead is of utmost importance in the perovskite research domain[79,80]. In this regard, quasi-2DP using Sn in replacement to Pb have been shown in the form of $PEA_2FA_{n-1}Sn_nI_{3n+1}$ bulk heterojunction film (see cartoon in Figure 6d)[81]. When mixed, the 2D phase segregates on the bottom of the 3D, forming a layered and highly oriented structure. PEA molecules infiltrate at the boundary of perovskite grains forming a compact pinhole-free films. This blocks the oxygen diffusion into the perovskite lattice, enhancing the stability. In addition, the perpendicular growth of the highly-oriented film improves the carrier transport. This film structure delivers modest performance (up to 6% PCE) and enhanced stability sustained over 100 h in nitrogen filled atmosphere. $(BA)_2(MA)_{n-1}Sn_nI_{3n+1}$ have been also developed with promising PCE of 2.5% for n = 4, stable for more than 1 month upon encapsulation (by thermally sealing a glass slide on top of the solar cell device at 115 °C using a 30 µm thick polymer) [82]. Histammonium (HA) dication and the benzylammonium (Bz) cation (Figure 6c) have been also used, forming $(HA)Pb_{1-x}Sn_xI_4$ and $(BzA)_2Pb_{1-x}Sn_xI_4$ perovskites[83]. Interestingly, for the pure n = 1 2DP, the Sn-based inorganic frameworks are rather undistorted. This results in slightly lower band gaps with respect to common lead-based 2DP[80].$(HA)SnI_4$ has a band gap of 1.67 eV while for $(HA)PbI_4$ it is 2.05 eV. For $(HA)PbI_4$ solar cells reach a high PCE of 1.13%[83]. On the other side, n>1 quasi-2DP demonstrated a record efficiency of 5.94% stable for over 100h without encapsulation.

4.5. Photophysics of quasi-2D and 2D/3D hybrids.

The understanding of the photophysical processes behind 2D/3D hybrid system has not grown at the same pace as the device engineering field. It is worth mentioning, first of all, that in the combined 2D/3D system, depending on the relative energy level alignment, different processes can happen. As depicted in Figure 7a, electron transfer from 2DP to 3DP or energy transfer from 2D to 3D component can occur. So far, the deep elucidation of these dynamical processes is still missing, keeping many different scenarios still open. In our work describing the 2D/3D junction made of $AVAPbI_4$ and $MAPbI_3$, we reported the theoretical model for the 2D/3D interface energy levels. We found that the 2D layer constitutes a barrier towards interfacial electron recombination, since the 2D CB lies at lower energy than that of the 3D CB, while favouring electron transfer to the TiO_2. However, experimental analysis on the photoinduced dynamics behind the 2D/3D interface is still undergoing. On the other side, few recent papers focused on the photophysics of quasi-2D systems which form multi-phases, as depicted in Figure 7c. This results into a multi- band gap material where charge or energy transfer across the film can happen[84,85]. According to the energy level alignment between the quasi-2DP with different n (see Figure 1e), charge transfer can happen from the pure 2D (with small n) to the adjacent thick layer phase (i.e., large n). Such charge transfer process has been observed by TAS to be extremely efficient (happening in ≈0.5 ps), ultimately leading to exciton localization at the smallest band gap 2DP (n > 5),

which can be faster than exciton or charge recombination. More in detail, charge transfer can be observed by monitoring the resulting photobleaching feature in the TA spectra at the exciton resonances (for n=1, 2, 3,..) and its subsequent dynamical evolution. For instance, upon charge transfer from 2DP with n=1 to n=2, the photobleaching signal relative to the exciton bleach at the n=1 resonance decreases, feeding the rise of the photobleaching at the n=2 exciton resonance within the same time scale (Figure 7e, f)[29,84,86,87]. Notably, the timescale of internal charge transfer is dominated by the geometries of the perovskites phases, their intermixing and the length over which phase separation occurs. If the phases (with different n) are largely separated, internal exciton/charge diffusion also happens before being transferred to the adjacent phase over a hundreds of ps timescale. In addition, the spatial location of the 2D and 3D phases strongly affects the charge dynamics. It has been recently shown, for instance, that in a typical $BA_2MA_{n-1}PbnI_{3n+1}$ 2DP, transient PL combined with TAS revealed that the small-n phases are primarily located at the bottom surface while the large-n phase reside at the upper surface of the film[88]. In this regard, electron and hole transfers occurred vertically in the opposite direction according to the energy alignment as shown in Figure 7d. Thus, internal charge separation happens and electron and holes can accumulate on the spatially separated upper and bottom surfaces of perovskite film, respectively. From this understanding, optimized material growth and interface and device engineering can be developed in a smart way taking benefit from the internal charge transfer dynamics. For instance, Quan et al. have recently tailored the composition of quasi-2DP based on $PEA_2(MA)_{n-1}Pb_nI_{3n+1}$ manipulating the different phases within the samples to direct energy transfer into the lowest-bandgap minority phase (see cartoon in Figure 7b)[29]. In this way, energy transfer prevails and thus radiative recombination outcompetes the nonradiative losses. Given the multiple band gap across the film, to discern the local dynamics photoluminescence microscopy has been also used to monitor quasi-2DP. For instance, a spatial distribution of the photoexcited species, both excitons and free carriers, have been observed in $(BA)_2(MA)_{n-1}Pb_nI_{3n+1}$ perovskites [84]. In this case, “edge states” at the interface of the perovskite grains have been highlighted. These states would then result beneficial for exciton dissociation into free carriers which are expected to be protected from non-radiative decay mechanisms such as electron–phonon coupling or electronic impurities. Within this model, the photogenerated excitons are able to diffuse to the edge of the crystallite. At the edge energy is transferred to edge traps which can then efficiently emit light more in the red [84]. In addition, weak trapping has been observed, turning into a positive effect to enhance the photocurrent in solar cells. Although interesting, much further work has to be done to explore the nature of those “edge” states, and to evaluate the real fraction of the exciton population which can dissociate into free charges in relation with the sample structure (number of layers n).

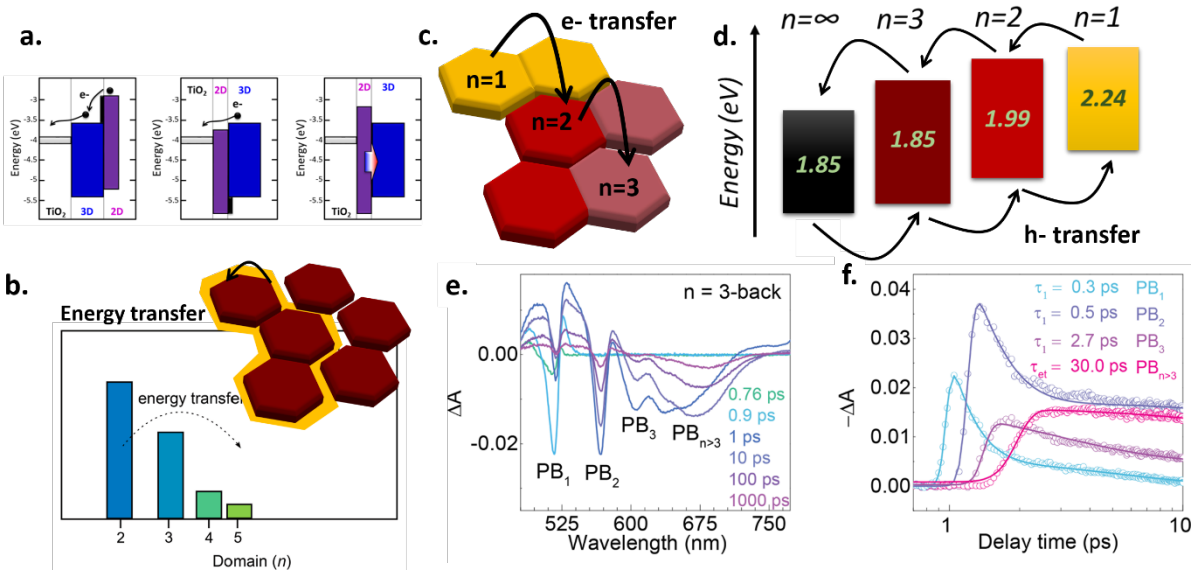

Figure 7. Photophysics of 2D and 2D/3D. a. Energy levels diagram showing the combined use of 2D and 3D perovskite, depending on the relative energy level alignment. **b.** 2D perovskite used at the border of the 3D perovskite crystal with proper energy match to favor energy transfer. Data reproduced from [Quan L.N. Nano Lett. 2017, 17, 3701]. **c.** scheme of a mixed phases sample with different quasi 2D perovskite (with different n), among which electron and hole transfer can happen. **d.** energy levels scheme showing 3D, quasi 2D and 2D perovskite and charge transfer dynamics. In a mixed-phase perovskite electron transfer happens from n=1 to n=∞ and vice versa for the hole transfer. **e.** Transient Absorption measurement showing the electron transfer process in a mixed phase compound and relative dynamics at selected probe wavelengths (**f.**). Data reproduced from [Shang Q. et al. J. Phys. Chem. Lett., 2017, 8, 4431].

4.6. Mobility and Diffusion Length of quasi-2DP.

Unveiling charge carrier mobility, charge carrier recombination rates and diffusion length as a function of the amount of 2D in the mixed system is paramount for device optimization. To this regard, Milot et al[89] have recently shown a comprehensive work on $MAPbI_3$, $(PEA)_2PbI_4$, and intermediate mixed MA–PEA 2DPs. It has been observed that the effective charge-carrier mobility generally decreases with increasing PEA content from 25 $cm^2 V^{-1}s^{-1}$ for $MAPbI_3$ to 1 $cm^2 V^{-1}s^{-1}$ for $(PEA)_2PbI_4$ due to the concomitant increase in the charge-carrier confinement and exciton binding energy with %PEA. Interestingly, the mobilities of the MA–PEA mixtures have been measured between 6 and 11 $cm^2 V^{-1}s^{-1}$, are remarkably good, comparable to the ones of working 3DP. Notably, if the fraction of the PEA is more than 50%, the 2D character (i.e. high exciton binding energy) dominates, reducing the benefit from the improved crystal orientation and charge mobility. The highest value has been obtained with 50% PEA, a record for 2DP. This is due to a concomitant effect of improved film quality

and morphology as well as diminished monomolecular recombination rate. This has been monitored by means of intensity dependent time resolved PL combined with optical pump- THz probe and fitted according to the following model $\frac{dn}{dt} = -k_3 n^3 - k_2 n^2 - k_1 n$ to retrieve the monomolecular (k_1), bimolecular (k_2) rate constant (n=charge carrier density). Compared to $MAPbI_3$ (k_1=1.3 × 10^7 s^{-1}), for 50% PEAI k_1 is reduced to 3.7 × 10^6 s^{-1} while increased up again to 1.1 × 10^9 s^{-1} for $(PEA)_2PbI_4$, due to exciton recombination. In parallel, charge diffusion length decreases with increasing %PEA (from 2.2 µm for $MAPbI_3$ to 60 nm for PEA_2PbI_4) due to the decrease of the charge-carrier mobility and the increased excitonic effects with PEA fraction. For 50%PEA, a maximum in charge-carrier diffusion length is reached, at 2.5 µm, which is higher than many reported values for even the 3DP[89]. More advanced studies on recombination rate and mobility in quasi-2DP using time-resolved microwave conductivity (TRMC) measurements have been performed by Venkatesan et al. on thin films of $BA_2MA_{n-1}Pb_nI_{3n+1}$[90]. Trap-assisted recombination has been found also in this sample as the main limit for carrier diffusion length and mobility. They found that the average recombination rate increases with n and that the yield−mobility products and carrier lifetimes of these thin films are even two order of magnitudes lower than the 3DP. Despite this introduces some discrepancies with other works, a lot of attention has to be focused on the 2D film morphology, crystalline texture and direction of growth, which dramatically changes the optoelectronic properties of the film. Pure 2D perovskite (i.e. n=1) display strong excitonic behaviour and low charge transport across the organic barrier, which might not be ideal ofr vertical charge transport in solar cell devices. Another example on TRMC measurements on a similar system has been reported by Gélvez-Rueda et al. [89] aiming to demonstrate the interconversion between bound excitons and free charges as a function of temperature. A clear increase of the charge mobility, along with enhanced probability of exciton dissociation, and of charge lifetime has been demonstrated with the increase of the number n layers, due to increased dielectric shielding of the electron−hole interactions.

5. Future perspectives.

The main drawback of the low-dimensional perovskites is charge transport, which is confined within the inorganic layer, where the organic cation forms a barrier resulting a quantum well structure. Also, the absorption of these materials is limited to a narrow region typically below 500nm, yielding reduced photocurrent and the power conversion efficiency compared to the 3D perovskites. The non-communicating cations such as butyl ammonium, phenylethylammonium, 5-aminovaleric acid [Giulia], and alkyl phosphonic acid, [Li X] form an insulating layer hindering photo-generated carrier

transportation that require out of the plane film growth leading a well aligned two- and three-dimensional perovskites. The perpendicularly orientated 2D inorganic framework to the 3D perovskite is essential for transporting photo-generated carriers to the contact. To increase further the charge transporting properties of the low-dimensional perovskites incorporating molecularly engineered cations with the ability of π-π stacking is vital. Tuning bandgap of the engineered cations, their optical properties, and energy levels to create an ideal sharp 2D/3D/2D interface are expected to take advantage of both the stability and efficiency. Specifically, the tailored organic cations that contribute energy alignment with the inorganic framework of 2D perovskite by modulating the highest occupied molecular orbitals (HOMO) and the lowest unoccupied molecular orbitals (LUMO) of the organic cations is paramount to enhance the power conversion efficiency. The other possible approach to enhance the stability of the 3D perovskite is the incorporation of polymerizable functional groups in 2D perovskite cations. This novel strategy opens a new field of possibilities, moving from a uniform 3D to a gradually structured 2D/3D/2D perovskites. The encapsulated 3D perovskite between polymer 2D perovskite layers is expected to exhibit increased efficiency and moisture stability. Also, a synergetic approach while keeping the high efficiency of the 3D perovskites and encapsulating with 2D perovskite layer at the bottom and on top will lead to best of both high efficiency and stability. The tailored cations are expected to stabilize lead iodide perovskite by stronger hydrogen bonding coupled with π-π stacking interaction of the cations. It is known that the cubic phase of α-CsPbI3 and α-FAPbI3 are thermodynamically unstable at room temperature where the former undergoes δ phase at below 320°C, and the later converts into non-perovskite yellow hexagonal δ-FAPbI3 phase. Since, the α-FAPbI3 perovskite has excellent absorption properties with 1.5 eV band gap, which can be stabilized by incorporating a rigid polymer 2D perovskite on the top and at the bottom preventing the conversion of the α-FAPbI3 phase into δ-FAPbI3 phase. The stabilized small bandgap α-FAPbI3 cubic phase will be a breakthrough in perovskite photovoltaics. Further advances in performance can also be achieved by optimizing the two-dimensional perovskites that transport positive charges by optimizing the HOMO levels of 2D perovskite and block electrons at the interface between the 3D perovskite and hole transporting material. Controlling the LUMO levels of the 2D perovskite requires meticulous selection of functional donor groups on the cations. Similarly, by inserting 2D perovskite between the electron transporting layer and the 3D perovskite where the LUMO levels of the 2D perovskite have to be aligned with the conduction band of 3D perovskite and electron transporting layer. Here lowering the LUMO levels can be realized by substituting electron acceptor groups on the cation.

Photoluminescence (PL) intensity of 2D perovskites is significantly higher than the 3D perovskites because of increased exciton binding energy and quantum well structure. The prospects to enhance PL intensity is excellent in 2 D perovskites with tailored cations, which themselves, for example, are

highly luminescent. Luminescent cations containing 2D perovskites can transfer energy from 2D to 3D perovskites that would be another interesting approach to harvest high energy photons and to enhance the efficiency and stability. Development of tailored 2D perovskites with suitable HOMO and LUMO energy levels will have remarkable implications in various applications that include light-emitting diodes, display, lasers, photodetectors, and X-ray imaging beyond the stable perovskite solar cells. Thus, following these multiple research directions, the future of 2D and 3D perovskites is bright where the 2D perovskite acts as a protecting layer on the bottom and the top of 3D perovskite absorber.

Moisture stability is greatly enhanced in 2DP and motivates the deep research in the field, however, one should also be aware that light-induced degradation can happen in 2DP lattice. This occurs via the release of the organic cation and HI as byproducts, mainly happening from the edges of the 2D crystals and the surfaces, where the inorganic layers are separated by the organics. This aspect, still not discussed enough in the 2D perovskite research can be a bottleneck for 2D perovskite device which must attract future attention.

To reach the above mentioned goals, more work has to be done to underpin the actual photophysics of 2DP and mixed 2D/3D to drive an intelligent device development. In particular, major breakthroughs are expected in the field of: i) material design and engineering aiming to replace the use of lead, which nowadays restrict the market application, going beyond the material library available so far; ii) deposition protocol optimization. Further work has to be done to deeply elucidate the relationship between structure, film quality and purity of phase dimensionality, and charge transport. This can be targeted by monitoring the fine structure determination with XRD and GIXRD, combined with advanced studies on the surface properties of the perovskite film, aiming to reveal the relationship between surface defects and structure stability via scanning tunnelling microscopy at a nanoscale level, as well as the surface structure effect on the performance of perovskite solar cell. However, its spatial resolution is still a limitation for fine structure characterization. Consequently, substantial development of fine-structure characterization approaches will also be needed, especially in in-situ and operando conditions to monitor the perovskite instability. Synchrotron-based scanning transmission electron microscopy can be a very helpful tool for both fine structure mapping and spatial element identification. X-ray fine structure absorption spectroscopy (XAFS) could also be considerably employed in the future to characterize the detailed information behind crystal structure, such as the exact coordination information of metal ions in the hybridized perovskite structure, the bonding length, and the chemical state as-prepared and under operando situation. Besides XAFS, the promotion of other structure characterization methods under operando conditions is an appealing direction for research that should not be ignored. One possible way could be the combination of

absorption spectroscopy and electrical measurements, by combining X-ray photoelectron spectroscopy (XPS) together with ultraviolet photoelectron spectroscopy (UPS) to determine surface and interface electronic structure and connect them to the electrical properties of perovskite solar cells

Beyond material and interface characterization , upscaling, and invention of low-cost deposition protocol (i.e. by printing technologies) should also be addressed. In conclusion, this work summarized the incredible evolution of 2DP and suggests a bright future for their use in high-tech optoelectronics industry. On the other side, further exploration of this class of materials is now urgent bridging together research efforts in chemistry, material science, physics, and device engineering.

References

1. Green, M. A. & Ho-Baillie, A. Perovskite Solar Cells: The Birth of a New Era in Photovoltaics. *ACS Energy Lett.* **2,** 822–830 (2017).
2. *http://www.nrel.gov/ncpv/images/efficiency_chart.jpg.*
3. Correa-Baena, J.-P. *et al.* Promises and challenges of perovskite solar cells. *Science* **358,** 739–744 (2017).
4. Saliba, M. Perovskite solar cells must come of age. *Science* **359,** 388–389 (2018).
5. Grätzel, M. The Rise of Highly Efficient and Stable Perovskite Solar Cells. *Acc. Chem. Res.* **50,** 487–491 (2017).
6. Wang, D., Wright, M., Elumalai, N. K. & Uddin, A. Stability of perovskite solar cells. *Sol. Energy Mater. Sol. Cells* **147,** 255–275 (2016).
7. Misra, R. K., Cohen, B.-E., Iagher, L. & Etgar, L. Low-Dimensional Organic–Inorganic Halide Perovskite: Structure, Properties, and Applications. *ChemSusChem* **10,** 3712–3721 (2017).
8. Stoumpos, C. C. *et al.* Ruddlesden–Popper Hybrid Lead Iodide Perovskite 2D Homologous Semiconductors. *Chem. Mater.* **28,** 2852–2867 (2016).
9. Tsai, H. *et al.* High-efficiency two-dimensional Ruddlesden–Popper perovskite solar cells. *Nature* **536,** 312–316 (2016).

10. Chen, Y. *et al.* 2D Ruddlesden–Popper Perovskites for Optoelectronics. *Adv. Mater.* n/a-n/a doi:10.1002/adma.201703487
11. Grancini, G. *et al.* One-Year stable perovskite solar cells by 2D/3D interface engineering. *Nat. Commun.* **8,** ncomms15684 (2017).
12. Taek Cho, K. *et al.* Selective growth of layered perovskites for stable and efficient photovoltaics. *Energy Environ. Sci.* (2018). doi:10.1039/C7EE03513F
13. Smith, I. C., Hoke, E. T., Solis-Ibarra, D., McGehee, M. D. & Karunadasa, H. I. A Layered Hybrid Perovskite Solar-Cell Absorber with Enhanced Moisture Stability. *Angew. Chem. Int. Ed.* **53,** 11232–11235 (2014).
14. Snaith, H. J. Perovskites: The Emergence of a New Era for Low-Cost, High-Efficiency Solar Cells. *J. Phys. Chem. Lett.* **4,** 3623–3630 (2013).
15. Kieslich, G., Sun, S. & Cheetham, A. K. Solid-state principles applied to organic–inorganic perovskites: new tricks for an old dog. *Chem. Sci.* **5,** 4712–4715 (2014).
16. D'Innocenzo, V. *et al.* Excitons versus free charges in organo-lead tri-halide perovskites. *Nat. Commun.* **5,** (2014).
17. Slavney, A. H. *et al.* Chemical Approaches to Addressing the Instability and Toxicity of Lead–Halide Perovskite Absorbers. *Inorg. Chem.* **56,** 46–55 (2017).
18. Berhe, T. A. *et al.* Organometal halide perovskite solar cells: degradation and stability. *Energy Environ. Sci.* **9,** 323–356 (2016).
19. You, J. *et al.* Improved air stability of perovskite solar cells via solution-processed metal oxide transport layers. *Nat. Nanotechnol.* **11,** 75–81 (2016).
20. Bella, F. *et al.* Improving efficiency and stability of perovskite solar cells with photocurable fluoropolymers. *Science* **354,** 203–206 (2016).
21. Li, X. *et al.* Improved performance and stability of perovskite solar cells by crystal crosslinking with alkylphosphonic acid ω-ammonium chlorides. *Nat. Chem.* **7,** 703–711 (2015).

22. Cao, D. H., Stoumpos, C. C., Farha, O. K., Hupp, J. T. & Kanatzidis, M. G. 2D Homologous Perovskites as Light-Absorbing Materials for Solar Cell Applications. *J. Am. Chem. Soc.* **137,** 7843–7850 (2015).

23. Saparov, B. & Mitzi, D. B. Organic–Inorganic Perovskites: Structural Versatility for Functional Materials Design. *Chem. Rev.* **116,** 4558–4596 (2016).

24. Du, K. *et al.* Two-Dimensional Lead(II) Halide-Based Hybrid Perovskites Templated by Acene Alkylamines: Crystal Structures, Optical Properties, and Piezoelectricity. *Inorg. Chem.* (2017). doi:10.1021/acs.inorgchem.7b01094

25. Dohner, E. R., Jaffe, A., Bradshaw, L. R. & Karunadasa, H. I. Intrinsic White-Light Emission from Layered Hybrid Perovskites. *J. Am. Chem. Soc.* **136,** 13154–13157 (2014).

26. Cho, H. *et al.* Overcoming the electroluminescence efficiency limitations of perovskite light-emitting diodes. *Science* **350,** 1222–1225 (2015).

27. Quan, L. N. *et al.* Ligand-Stabilized Reduced-Dimensionality Perovskites. *J. Am. Chem. Soc.* **138,** 2649–2655 (2016).

28. Kamminga, M. E. *et al.* Confinement Effects in Low-Dimensional Lead Iodide Perovskite Hybrids. *Chem. Mater.* **28,** 4554–4562 (2016).

29. Quan, L. N. *et al.* Tailoring the Energy Landscape in Quasi-2D Halide Perovskites Enables Efficient Green-Light Emission. *Nano Lett.* **17,** 3701–3709 (2017).

30. Braun, M., Tuffentsammer, W., Wachtel, H. & Wolf, H. C. Tailoring of energy levels in lead chloride based layered perovskites and energy transfer between the organic and inorganic planes. *Chem. Phys. Lett.* **303,** 157–164 (1999).

31. Mitzi, D. B. Synthesis, Structure, and Properties of Organic-Inorganic Perovskites and Related Materials. in *Progress in Inorganic Chemistry* (ed. Karlin, K. D.) 1–121 (John Wiley & Sons, Inc., 1999).

32. Younts, R. *et al.* Efficient Generation of Long-Lived Triplet Excitons in 2D Hybrid Perovskite. *Adv. Mater.* **29,** n/a-n/a (2017).

33. Era, M., Hattori, T., Taira, T. & Tsutsui, T. Self-Organized Growth of PbI-Based Layered Perovskite Quantum Well by Dual-Source Vapor Deposition. *Chem. Mater.* **9,** 8–10 (1997).
34. Mitzi, D. B. A Layered Solution Crystal Growth Technique and the Crystal Structure of (C6H5C2H4NH3)2PbCl4. *J. Solid State Chem.* **145,** 694–704 (1999).
35. Cortecchia, D. *et al.* Broadband Emission in Two-Dimensional Hybrid Perovskites: The Role of Structural Deformation. (2016). Available at: https://pubs.acs.org/doi/abs/10.1021/jacs.6b10390. (Accessed: 23rd March 2018)
36. and, J. L. K., Martin*, J. D. & Mitzi, D. B. Tuning the Band Gap in Hybrid Tin Iodide Perovskite Semiconductors Using Structural Templating. (2005). Available at: https://pubs.acs.org/doi/abs/10.1021/ic050244q. (Accessed: 23rd March 2018)
37. Wu, X., Trinh, M. T. & Zhu, X.-Y. Excitonic Many-Body Interactions in Two-Dimensional Lead Iodide Perovskite Quantum Wells. *J. Phys. Chem. C* **119,** 14714–14721 (2015).
38. Poglitsch, A. & Weber, D. Dynamic disorder in methylammoniumtrihalogenoplumbates (II) observed by millimeter-wave spectroscopy. *J. Chem. Phys.* **87,** 6373–6378 (1987).
39. Anderson, P. W. Absence of Diffusion in Certain Random Lattices. *Phys. Rev.* **109,** 1492–1505 (1958).
40. Grancini, G. *et al.* Role of microstructure in the electron–hole interaction of hybrid lead halide perovskites. *Nat. Photonics* **9,** 695–701 (2015).
41. Peyghambarian, N. *et al.* Blue Shift of the Exciton Resonance due to Exciton-Exciton Interactions in a Multiple-Quantum-Well Structure. *Phys. Rev. Lett.* **53,** 2433–2436 (1984).
42. Hulin, D. *et al.* Well-size dependence of exciton blue shift in GaAs multiple-quantum-well structures. *Phys. Rev. B* **33,** 4389–4391 (1986).
43. Cortecchia, D. *et al.* Polaron self-localization in white-light emitting hybrid perovskites. *J. Mater. Chem. C* **5,** 2771–2780 (2017).
44. Hu, T. *et al.* Mechanism for Broadband White-Light Emission from Two-Dimensional (110) Hybrid Perovskites. *J. Phys. Chem. Lett.* **7,** 2258–2263 (2016).

45. Neogi, I. *et al.* Broadband-Emitting 2 D Hybrid Organic–Inorganic Perovskite Based on Cyclohexane-bis(methylamonium) Cation. *ChemSusChem* **10,** 3765–3772 (2017).
46. Yangui, A. *et al.* Optical Investigation of Broadband White-Light Emission in Self-Assembled Organic–Inorganic Perovskite (C6H11NH3)2PbBr4. *J. Phys. Chem. C* **119,** 23638–23647 (2015).
47. Ohnishi, A., Tanaka, K. & Yoshinari, T. Exciton Self-Trapping in Two-Dimensional System of (C 2H 5NH 3) 2CdCl 4 Single Crystal. *J. Phys. Soc. Jpn.* **68,** 288–290 (1999).
48. Manchon, A., Koo, H. C., Nitta, J., Frolov, S. M. & Duine, R. A. New perspectives for Rashba spin–orbit coupling. *Nat. Mater.* **14,** 871–882 (2015).
49. Dresselhaus, G., Kip, A. F. & Kittel, C. Spin-Orbit Interaction and the Effective Masses of Holes in Germanium. *Phys. Rev.* **95,** 568–569 (1954).
50. Zhai, Y. *et al.* Giant Rashba splitting in 2D organic-inorganic halide perovskites measured by transient spectroscopies. *Sci. Adv.* **3,** e1700704 (2017).
51. Aristidou, N. *et al.* Fast oxygen diffusion and iodide defects mediate oxygen-induced degradation of perovskite solar cells. *Nat. Commun.* **8,** 15218 (2017).
52. De Bastiani, M. *et al.* Ion migration and the role of preconditioning cycles in the stabilization of the J–V characteristics of inverted hybrid perovskite solar cells. *Adv. Energy Mater.* **6,** (2016).
53. Bi, E. *et al.* Diffusion engineering of ions and charge carriers for stable efficient perovskite solar cells. *Nat. Commun.* **8,** ncomms15330 (2017).
54. Gratia, P. *et al.* Intrinsic Halide Segregation at Nanometer Scale Determines the High Efficiency of Mixed Cation/Mixed Halide Perovskite Solar Cells. *J. Am. Chem. Soc.* **138,** 15821–15824 (2016).
55. Leijtens, T. *et al.* Mapping Electric Field-Induced Switchable Poling and Structural Degradation in Hybrid Lead Halide Perovskite Thin Films. *Adv. Energy Mater.* **5,** (2015).
56. Yang, Y. & You, J. Make perovskite solar cells stable. *Nat. News* **544,** 155 (2017).
57. McMeekin, D. P. *et al.* A mixed-cation lead mixed-halide perovskite absorber for tandem solar cells. *Science* **351,** 151–155 (2016).

58. Saliba, M. *et al.* Incorporation of rubidium cations into perovskite solar cells improves photovoltaic performance. *Science* **354,** 206–209 (2016).

59. Zhang, Y., Grancini, G., Feng, Y., Asiri, A. M. & Nazeeruddin, M. K. Optimization of Stable Quasi-Cubic FAxMA1–xPbI3 Perovskite Structure for Solar Cells with Efficiency beyond 20%. *ACS Energy Lett.* **2,** 802–806 (2017).

60. Jodlowski, A. D. *et al.* Large guanidinium cation mixed with methylammonium in lead iodide perovskites for 19% efficient solar cells. *Nat. Energy* **2,** 972–979 (2017).

61. Soe, C. M. M. *et al.* New Type of 2D Perovskites with Alternating Cations in the Interlayer Space, (C(NH2)3)(CH3NH3)nPbnI3n+1: Structure, Properties, and Photovoltaic Performance. (2017). Available at: https://pubs.acs.org/doi/abs/10.1021/jacs.7b09096. (Accessed: 23rd March 2018)

62. Domanski, K. *et al.* Not All That Glitters Is Gold: Metal-Migration-Induced Degradation in Perovskite Solar Cells. *ACS Nano* **10,** 6306–6314 (2016).

63. Mei, A. *et al.* A hole-conductor–free, fully printable mesoscopic perovskite solar cell with high stability. *Science* **345,** 295–298 (2014).

64. Wang, Z. *et al.* Efficient ambient-air-stable solar cells with 2D–3D heterostructured butylammonium-caesium-formamidinium lead halide perovskites. *Nat. Energy* **2,** nenergy2017135 (2017).

65. Chen Yani *et al.* Tailoring Organic Cation of 2D Air-Stable Organometal Halide Perovskites for Highly Efficient Planar Solar Cells. *Adv. Energy Mater.* **7,** 1700162 (2017).

66. Iagher, L. & Etgar, L. Effect of Cs on the Stability and Photovoltaic Performance of 2D/3D Perovskite-Based Solar Cells. *ACS Energy Lett.* 366–372 (2018). doi:10.1021/acsenergylett.7b01196

67. Jiang, W. *et al.* A new layered nano hybrid perovskite film with enhanced resistance to moisture-induced degradation. *Chem. Phys. Lett.* **658,** 71–75 (2016).

68. Cohen, B.-E., Wierzbowska, M. & Etgar, L. High efficiency quasi 2D lead bromide perovskite solar cells using various barrier molecules. *Sustain. Energy Fuels* **1,** 1935–1943 (2017).

69. Cohen Bat-El, Wierzbowska Małgorzata & Etgar Lioz. High Efficiency and High Open Circuit Voltage in Quasi 2D Perovskite Based Solar Cells. *Adv. Funct. Mater.* **27,** 1604733 (2016).

70. Yao, K., Wang, X., Li, F. & Zhou, L. Mixed perovskite based on methyl-ammonium and polymeric-ammonium for stable and reproducible solar cells. *Chem. Commun.* **51,** 15430–15433 (2015).

71. Yao, K., Wang, X., Xu, Y., Li, F. & Zhou, L. Multilayered Perovskite Materials Based on Polymeric-Ammonium Cations for Stable Large-Area Solar Cell. *Chem. Mater.* **28,** 3131–3138 (2016).

72. Koh, T. M. *et al.* Nanostructuring Mixed-Dimensional Perovskites: A Route Toward Tunable, Efficient Photovoltaics. *Adv. Mater.* **28,** 3653–3661 (2016).

73. Ma, C. *et al.* 2D/3D perovskite hybrids as moisture-tolerant and efficient light absorbers for solar cells. *Nanoscale* **8,** 18309–18314 (2016).

74. Lin, Y. *et al.* Enhanced Thermal Stability in Perovskite Solar Cells by Assembling 2D/3D Stacking Structures. *J. Phys. Chem. Lett.* (2018). doi:10.1021/acs.jpclett.7b02679

75. Chen Jiangzhao, Seo Ja-Young & Park Nam-Gyu. Simultaneous Improvement of Photovoltaic Performance and Stability by In Situ Formation of 2D Perovskite at (FAPbI3)0.88(CsPbBr3)0.12/CuSCN Interface. *Adv. Energy Mater.* **0,** 1702714 (2018).

76. Chen, J., Lee, D. & Park, N.-G. Stabilizing the Ag Electrode and Reducing J–V Hysteresis through Suppression of Iodide Migration in Perovskite Solar Cells. *ACS Appl. Mater. Interfaces* **9,** 36338–36349 (2017).

77. Lee, D. S. *et al.* Passivation of Grain Boundaries by Phenethylammonium in Formamidinium-Methylammonium Lead Halide Perovskite Solar Cells. *ACS Energy Lett.* 647–654 (2018). doi:10.1021/acsenergylett.8b00121

78. Koh, T. M. *et al.* Enhancing moisture tolerance in efficient hybrid 3D/2D perovskite photovoltaics. *J. Mater. Chem. A* **6,** 2122–2128 (2018).

79. Giustino, F. & Snaith, H. J. Toward Lead-Free Perovskite Solar Cells. *ACS Energy Lett.* **1,** 1233–1240 (2016).

80. Hao, F., Stoumpos, C. C., Cao, D. H., Chang, R. P. H. & Kanatzidis, M. G. Lead-free solid-state organic–inorganic halide perovskite solar cells. *Nat. Photonics* **8,** 489–494 (2014).

81. Ran, C. *et al.* Bilateral Interface Engineering toward Efficient 2D–3D Bulk Heterojunction Tin Halide Lead-Free Perovskite Solar Cells. *ACS Energy Lett.* (2018). doi:10.1021/acsenergylett.8b00085

82. Cao, D. H. *et al.* Thin Films and Solar Cells Based on Semiconducting Two-Dimensional Ruddlesden–Popper (CH3(CH2)3NH3)2(CH3NH3)n−1SnnI3n+1 Perovskites. *ACS Energy Lett.* **2,** 982–990 (2017).

83. Mao, L. *et al.* Role of Organic Counterion in Lead- and Tin-Based Two-Dimensional Semiconducting Iodide Perovskites and Application in Planar Solar Cells. *Chem. Mater.* **28,** 7781–7792 (2016).

84. Blancon, J.-C. *et al.* Extremely efficient internal exciton dissociation through edge states in layered 2D perovskites. *Science* eaal4211 (2017). doi:10.1126/science.aal4211

85. Pedesseau, L. *et al.* Advances and Promises of Layered Halide Hybrid Perovskite Semiconductors. *ACS Nano* **10,** 9776–9786 (2016).

86. Liao, Y. *et al.* Highly Oriented Low-Dimensional Tin Halide Perovskites with Enhanced Stability and Photovoltaic Performance. *J. Am. Chem. Soc.* **139,** 6693–6699 (2017).

87. Shang, Q. *et al.* Unveiling Structurally Engineered Carrier Dynamics in Hybrid Quasi-Two-Dimensional Perovskite Thin Films toward Controllable Emission. *J. Phys. Chem. Lett.* **8,** 4431–4438 (2017).

88. Liu, J., Leng, J., Wu, K., Zhang, J. & Jin, S. Observation of Internal Photoinduced Electron and Hole Separation in Hybrid Two-Dimentional Perovskite Films. *J. Am. Chem. Soc.* **139,** 1432–1435 (2017).

89. Gélvez-Rueda, M. C. *et al.* Interconversion between Free Charges and Bound Excitons in 2D Hybrid Lead Halide Perovskites. *J. Phys. Chem. C* **121,** 26566–26574 (2017).

90. Venkatesan, N. R., Labram, J. G. & Chabinyc, M. L. Charge-Carrier Dynamics and Crystalline Texture of Layered Ruddlesden–Popper Hybrid Lead Iodide Perovskite Thin Films. *ACS Energy Lett.* 380–386 (2018). doi:10.1021/acsenergylett.7b01245
91. La-Placa, M.-G. *et al.* Photoluminescence quantum yield exceeding 80% in low dimensional perovskite thin-films via passivation control. *Chem. Commun.* **53,** 8707–8710 (2017).
92. Yuan, Z. *et al.* One-dimensional organic lead halide perovskites with efficient bluish white-light emission. *Nat. Commun.* **8,** ncomms14051 (2017).
93. Matsushima Toshinori *et al.* Solution-Processed Organic–Inorganic Perovskite Field-Effect Transistors with High Hole Mobilities. *Adv. Mater.* **28,** 10275–10281 (2016).
94. Birowosuto, M. D. *et al.* X-ray Scintillation in Lead Halide Perovskite Crystals. *Sci. Rep.* **6,** (2016).
95. Subnanosecond time-resolved x-ray measurements using an organic-inorganic perovskite scintillator: Applied Physics Letters: Vol 93, No 26. Available at: https://aip.scitation.org/doi/abs/10.1063/1.3059562. (Accessed: 23rd March 2018)
96. Chanana, A. *et al.* Colour selective control of terahertz radiation using two-dimensional hybrid organic inorganic lead-trihalide perovskites. *Nat. Commun.* **8,** 1328 (2017).

Acknowledgements

The authors acknowledge SNSF NRP 70 project; number:407040_154056, and CTI 15864.2 PFNM-NM, Solaronix, Aubonne, Switzerland. G.G. acknowledges the Swiss National Science Foundation (SNSF) funding through the Ambizione Energy project HYPER (grant number PZENP2_173641). The authors thanks Dr. Sadig Aghazada for reading the manuscript and for providing useful discussion.